Recent developments in thermoelectric materials

G. Chen, M. S. Dresselhaus, G. Dresselhaus, J.-P. Fleurial and T. Caillat

Efficient solid state energy conversion based on the Peltier effect for cooling and the Seebeck effect for power generation calls for materials with high electrical conductivity σ, high Seebeck coefficient S, and low thermal conductivity k. Identifying materials with a high thermoelectric figure of merit $Z(=S^2\sigma/k)$ has proven to be an extremely challenging task. After 30 years of slow progress, thermoelectric materials research experienced a resurgence, inspired by the developments of new concepts and theories to engineer electron and phonon transport in both nanostructures and bulk materials. This review provides a critical summary of some recent developments of new concepts and new materials. In nanostructures, quantum and classical size effects provide opportunities to tailor the electron and phonon transport through structural engineering. Quantum wells, superlattices, quantum wires, and quantum dots have been employed to change the band structure, energy levels, and density of states of electrons, and have led to improved energy conversion capability of charged carriers compared to those of their bulk counterparts. Interface reflection and the scattering of phonons in these nanostructures have been utilised to reduce the heat conduction loss. Increases in the thermoelectric figure of merit based on size effects for either electrons or phonons have been demonstrated. In bulk materials, new synthetic routes have led to engineered complex crystal structures with the desired phonon–glass electron–crystal behaviour. Recent studies on new materials have shown that dimensionless figure of merit ($Z\times$temperature) values close to 1·5 could be obtained at elevated temperatures. These results have led to intensified scientific efforts to identify, design, engineer and characterise novel materials with a high potential for achieving ZT much greater than 1 near room temperature. IMR/397

© Dr Chen is in the Mechanical Engineering Department, Massachusetts Institute of Technology, Cambridge, MA 02139, USA (gchen2@mit.edu). Dr M. S. Dresselhaus is in the Department of Physics, Department of Electrical Engineering and Computer Science, Massachusetts Institute of Technology, Cambridge, MA 02139, USA. Dr G. Dresselhaus is in the Francis Bitter Magnet Laboratory, Massachusetts Institute of Technology, Cambridge, MA 02139, USA. Dr Fleurial and Dr Caillat are in the Jet Propulsion Laboratory, California Institute of Technology, 4800 Oak Grove Drive, MS 277–207, Pasadena, CA 91109, USA.

List of symbols

C	phonon volumetric specific heat per unit frequency interval, J m^{-3} K^{-1} Hz^{-1}
E	electron energy, J
e	electron unit charge, C
F	Fermi–Dirac integral defined by equation (8)
f	distribution function
$\hbar$	Planck's coefficient divided by 2π, J s
I	current, A
k	thermal conductivity, W m^{-1} K^{-1}
k_B	Boltzmann's constant, J K^{-1}
L	functions defined by equation (4)
m^*	effective mass, kg
Q	heat current, W
S	Seebeck coefficient, V K^{-1}
T	temperature, K
V	voltage, V
$\mathbf{v}$	velocity, m s^{-1}
Z	figure of merit, K^{-1}
ZT	non-dimensional figure of merit
φ	azimuthal angle
θ	polar angle
Λ	mean free path, m
μ	chemical potential, J
ξ	chemical potential divided by $k_B T$
Π	Peltier coefficient, V
σ	electrical conductivity, S m
τ	relaxation time, s
ω	angular frequency, Hz rad

Introduction

Solid state cooling and power generation based on thermoelectric effects have been known since the Seebeck effect (for power generation) and the Peltier effect (for cooling and heat pumping) were discovered in the 1800s.[1] The Seebeck effect is associated with the generation of a voltage along a conductor when it is subjected to a temperature difference. Charged carriers (electrons or holes) diffuse from the hot side to the cold side, creating an internal electric field that opposes further diffusion. The Seebeck coefficient is defined as the voltage generated per degree of temperature difference between two points

$$S = -\frac{V_{12}}{\Delta T_{12}} \quad \ldots \quad (1)$$

The Peltier effect reflects the fact that when carriers flow through a conductor, they also carry heat. The heat current Q is proportional to the charge current I

$$Q = \Pi I \quad \ldots \quad (2)$$

and the proportionality constant Π is called the Peltier coefficient. When two materials are joined together and a current is passed through the interface, there will be an excess or deficiency in the energy at the junction because the two materials have different Peltier coefficients. The excess energy is released to the lattice at the junction, causing heating, and the deficiency in energy is supplied by the lattice, creating cooling. The Seebeck and the Peltier coefficients are related through the Kelvin relation $\Pi = ST$, where T is the absolute temperature.[1] A typical thermoelectric cooler is shown in Fig. 1*a*. P-type and n-type semi-

DOI 10.1179/095066003225010182

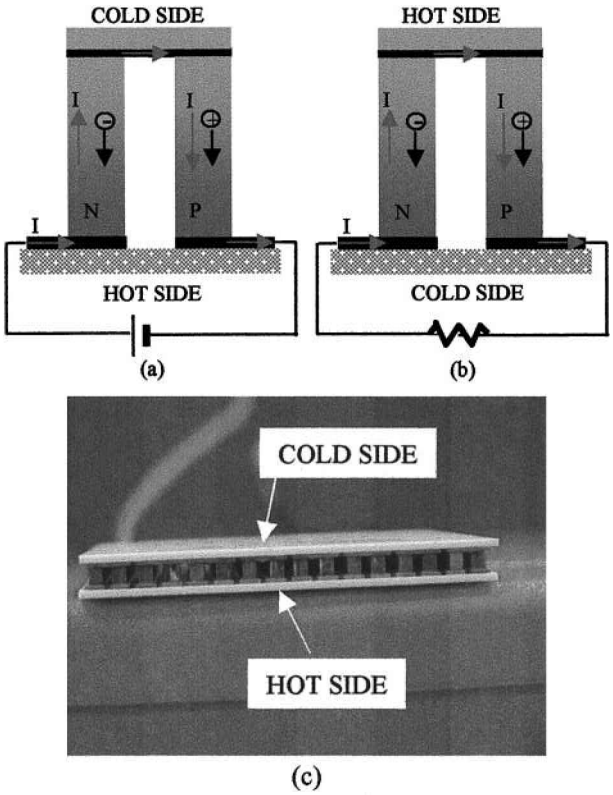

a cooler; *b* power generator; *c* actual device

1 Illustration of thermoelectric devices

conductor elements are interconnected on the cold and the hot sides, such that a current flows through all the elements in series, while the energy they carry (by electrons and holes) leaves the cold side in parallel. Thermoelectric power generators work in reverse to thermoelectric coolers, as shown in Fig. 1*b*. Because the hot side has a higher temperature, electrons and holes are driven to the cold side through diffusion and flow through an external load to do useful work. Practical devices are made of many pairs of p–n legs (Fig. 1*c*), usually arranged such that current flows in series through all the legs and energy flows in parallel from the cold side to the hot side.

In addition to the temperatures of the hot and cold sides, which are important to all thermal engines, the efficiency of actual thermoelectric devices is determined by the thermoelectric figure of merit

$$Z = \frac{S^2\sigma}{k} \quad . . . . . (3)$$

where σ is the electrical conductivity and k is the thermal conductivity. The appearance of S in Z is self-explanatory. The reason that the electrical conductivity σ enters Z is due to Joule heating. When a current passes through the thermoelectric elements, Joule heat is generated which can be conducted back to the cold junction. The thermal conductivity k appears in the denominator of Z because, in thermoelectric coolers or power generators, the thermoelectric elements also act as the thermal insulation between the hot and the cold sides. A high thermal conductivity causes too much heat leakage between the hot and the cold sides. The figure of merit Z has the units of inverse Kelvin and it often appears as a product with an absolute temperature T, such as the average device temperature. Thus, the dimensionless numerical figure of merit ZT is often cited rather than Z by itself.

The central issue in thermoelectrics materials research is to increase ZT. The best ZT materials are found in heavily doped semiconductors. Insulators have poor electrical conductivity. Metals have relatively low Seebeck coefficients. In addition, the thermal conductivity of a metal, which is dominated by electrons, is in most cases proportional to the electrical conductivity, as dictated by the Wiedmann–Franz law. It is thus hard to realise high ZT in metals. In semiconductors, the thermal conductivity has contributions from both electrons k_e and phonons k_p, with the majority usually coming from phonons. The phonon thermal conductivity can be reduced without causing too much reduction in the electrical conductivity. A proven approach to reduce the phonon thermal conductivity is through alloying.[2] The mass difference scattering in an alloy reduces the lattice thermal conductivity significantly without much degradation to the electrical conductivity. The commercial state of the art thermoelectric cooling materials are based on alloys of Bi_2Te_3 with Sb_2Te_3 (such as $Bi_{0.5}Sb_{1.5}Te_3$, p-type) and Bi_2Te_3 with Bi_2Se_3 (such as $Bi_2Te_{2.7}Se_{0.3}$, n-type), each having a ZT at room temperature approximately equal to 1. Refrigerators based on such materials typically have a coefficient of performance (COP) of about 1,[1] compared to compressor based refrigerators with a COP between 2 and 4 operating over a comparable working temperature range. Their low COP has limited thermoelectric coolers to niche market sectors, such as temperature stabilisation of semiconductor lasers and picnic coolers. The market for thermoelectric coolers, however, is rapidly increasing, partly due to the explosive growth of optical telecommunication. State of the art power generation materials are PbTe and $Si_{0.8}Ge_{0.2}$, which have been used in deep space radioisotope thermoelectric power generators that operate at $\sim$900°C with a maximum efficiency of about 7%.

From equation (3), one can infer that the best thermoelectric devices should have a thermal conductivity close to zero. One possibility is using vacuum between the cold and the hot side. Electrons can be emitted through a thermionic emission process from a metal surface and flow through a vacuum. This is the principle behind thermionic power generators, which were developed in the 1950s.[3] In a vacuum based thermionic power generator, the emitter is held at a high temperature. Electrons with energy higher than the work function can escape from the emitter surface and reach the collector. Conceivably, rather than for power generation, vacuum thermionic emission can also be used for cooling, if a current drives electrons from the emitter to the collector, as in a vacuum tube. The major problem, however, is that most metals have a large work function value, which makes room temperature refrigeration based on vacuum thermionic emission impractical.[4]

The progress since the 1960s in improving ZT had been very slow before the 1990s. The value of maximum ZT had essentially remained around 1 and

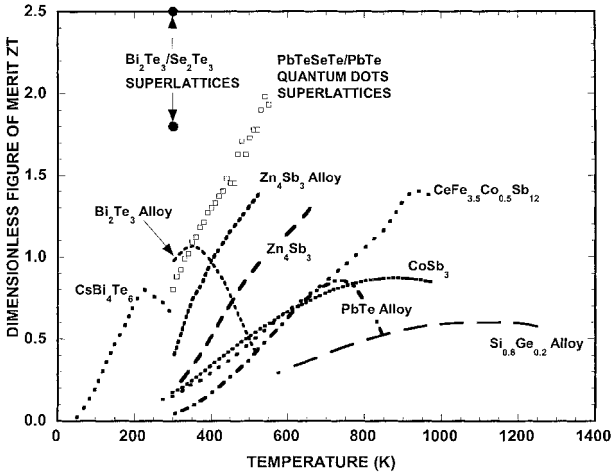

2 Non-dimensional figure of merit *ZT* as function of temperature for state of the art materials

research funding in this area dwindled. The landscape in thermoelectrics research changed quite significantly in the 1990s due to several new conceptual developments and renewed interested from several US research funding agencies. New developments occurred both in bulk materials and in low-dimensional materials. The best thermoelectric materials were succinctly summarised as 'phonon–glass electron–crystal' (or PGEC in short), which means that the materials should have a low lattice thermal conductivity as in a glass, and a high electrical conductivity as in crystals.[5] In bulk materials, the major new concept that was developed is the use of 'phonon rattlers' to reduce the lattice thermal conductivity. These phonon rattlers are normally interstitial atoms inserted into empty spaces in the host materials. Their vibration is not in harmony with the atoms in the host material, thus scattering the phonons in the original lattice. In this connection, several classes of materials have been discovered and/or re-investigated with regard to their potential for high ZT, such as skutterudites and clathrates. In low-dimensional materials, such as thin films, superlattices, and quantum wires, several approaches have been proposed. For transport along the film plane (wire axis) direction, quantum size effects are considered to increase the electronic power factor $S^2\sigma$ and boundary scattering to reduce k.[6,7] For transport in the direction perpendicular to the film plane, several possibilities were suggested. One was to use the band-edge discontinuity as a filter for cold electrons.[8] This was later developed into a thermionic emission cooling approach.[9,10] Another approach was based on phonon reflection at interfaces to reduce the lattice thermal conductivity.[11,12] Figure 2 shows a 'snapshot' of the reported ZT values. The ZT values of low-dimensional structures are subject to higher uncertainty and should be taken cautiously, primarily due to the difficulties involved in characterising the ZT of low-dimensional materials.

In this paper, it is intended to provide a concise critical review of some recent developments in thermoelectrics research. An extensive review of most of the topics discussed here is contained in a recently published three volume series.[13] A few other reviews and introductory reports have also been published, emphasising bulk thermoelectric materials.[14–17] Proceedings of International Conferences on 'Thermoelectrics',[18] which are held annually, and several volumes[19] of the MRS proceedings on this topic give broad coverage of progress made in recent years. This review is directed more towards low-dimensional materials, although bulk materials are also covered to provide readers with a quick overview of current thermoelectric materials research. The selection of the coverage was influenced by the research focus of the present authors and reflects their assessment of the field. The above mentioned references should be consulted for more comprehensive coverage.

Directions in search of high *ZT* materials

Expressions for thermoelectric properties are often derived from the Boltzmann equation under the relaxation time approximation[20]

$$\sigma = L^{(0)}, \quad k_e = \frac{L^{(2)}}{e^2 T} - \frac{L^{(1)}L^{(1)}}{e^2 T L^{(0)}}, \quad S = -\frac{L^{(1)}}{eTL^{(0)}} \tag{4}$$

where

$$L^{\alpha} = e^2 \int \frac{d^3\mathbf{k}}{4\pi^3} \left(-\frac{\partial f_{FD}}{\partial E}\right) \tau[E(\mathbf{k})][\mathbf{v}(\mathbf{k})]^2 [E(\mathbf{k}) - \mu]^{\alpha} \tag{5}$$

In the above expressions, f_{FD} is the Fermi–Dirac distribution, τ is the electron (hole) relaxation time, $\mathbf{k}$ is the electron wave vector, k_e is the electronic contribution to thermal conductivity, $\mathbf{v}$ is the electron group velocity, and e is the unit charge. If the relaxation time is assumed to be a constant and a three-dimensional (3D) parabolic electronic energy band is assumed, ZT can be expressed as[1,21]

$$Z_{3D}T = \frac{[(5F_{3/2}/3F_{1/2}) - \xi^*]^2 (3F_{1/2}/2)}{1/B_{3D} + 7F_{5/2}/2 - (25F_{3/2}^2/6F_{1/2})} \tag{6}$$

where

$$B_{3D} = \frac{(m^*)^{3/2}}{3\pi^2} \left(\frac{2k_B T}{\hbar^2}\right)^{3/2} \frac{k_B^2 T\mu}{ek_p} \tag{7}$$

and $m^* = (m_x m_y m_z)^{1/3}$ is the effective density of states mass of electrons in the band, k_p is the phonon contribution to the thermal conductivity, k_B is Boltzmann's constant, μ is the electron mobility, ξ^* is the chemical potential normalised by $k_B T$, and F_i is the Fermi–Dirac integral defined as

$$F_i(\xi^*) = \int_0^{\infty} \frac{x^i \, dx}{\exp(x - \xi^*) + 1} \tag{8}$$

In equations (6) and (7), the subscript 3D is used to indicate that those expressions are derived considering the density of states of 3D bulk crystals. In low-dimensional structures, these expressions must be reformulated.[21] In equation (6), the reduced chemical potential ξ^* is a free variable that can be controlled by doping. The optimum value for the chemical potential is chosen to maximise ZT. Therefore, thermoelectric materials development involves careful

control and optimisation of doping. The only other variable that affects the ZT value in equation (6) is the B factor, which depends on the electron effective mass, the carrier mobility, and the phonon thermal conductivity. The larger the B factor, the larger is ZT. Thus, thermoelectric materials research is often guided by finding materials that have a large B factor, which include a large electron (hole) effective mass and a high mobility, and a low lattice thermal conductivity. Such materials are succinctly called phonon–glass electron–crystal materials by Slack.[5] It should be pointed out that the requirements of a high mobility (which needs a low mobility effective mass) and a high density of states (which demands a large density of states effective mass) are not necessarily mutually exclusive. In anisotropic media, either in bulk form or in superlattices, it is possible to have a small effective mass in the current flow direction to give a high mobility and large effective masses in the directions perpendicular to the current flow to give a high density of states.

It should be mentioned that the derivation of equation (6) is based on the constant relaxation time approximation. A more realistic form of the relaxation time has an energy dependence $\tau \propto E^{\gamma}$, which depends on the scattering mechanisms. For example, $\gamma = 1/2$ for optical phonons, and $\gamma = -1$ for acoustic phonons.[1] It can be shown that ZT also depends on γ. Thus, one strategy that is sometimes used to improve ZT is to control the scattering mechanism.

The thermal conductivity of phonons is also often modelled from the Boltzmann equation under the relaxation time approximation, i.e.

$$k_{\mathrm{p}} = \sum_{\mathrm{p}} \int \frac{d^3\mathbf{k}}{8\pi^3} [\mathbf{v}_{\mathrm{p}x}(\mathbf{k})]^2 \frac{\partial f_{\mathrm{p}}}{\partial T} \tau_{\mathrm{p}} \hbar\omega$$

$$= \frac{1}{3} \int C(\omega) \mathbf{v}_{\mathrm{p}}(\omega) \Lambda_{\mathrm{p}}(\omega)\, \mathrm{d}\omega \quad . \quad . \quad . \quad . \quad . \quad . \quad (9)$$

for an isotropic bulk material, where f_{p} is the phonon distribution function, C is the specific heat of phonons at frequency ω, $\mathbf{v}_{\mathrm{p}}$ is the phonon group velocity, τ_{p} is the phonon relaxation time, Λ_{p} is the free path of phonons at ω and the summation is over the different phonon polarisations. To reduce the thermal conductivity, materials with a small phonon group velocity and a short relaxation time are desired. Roughly speaking, the phonon group velocity is proportional to $(K/m)^{1/2}$, where K is the spring constant between the atoms and m is the mass of the atom. Thus, materials with high atomic mass are often used for thermoelectric materials. The phonon relaxation time can be reduced by scattering, such as through alloying[2] and by adding phonon rattlers.[15]

Successful bulk thermoelectric materials that were developed in the past were directed by the principles derived from the above general discussion for bulk materials. For example, Bi_2Te_3 was tested because of its high atomic weight.[22] Other important characteristics of Bi_2Te_3 that were discovered later, such as its multiple carrier pockets, high mobility, and low thermal conductivity, all contributed to its high ZT value because all these factors work favourably to increase the B factor. In contrast, SiGe is not a high atomic weight material. Its success relies on its multiple carrier pockets that give a reasonably high density of states and, more importantly, on the alloying method that significant lowers its thermal conductivity compared to that of bulk Si or Ge. High temperature operation also helps to increase the ZT of $Si_{1-x}Ge_x$.

While the general ZT formulation for bulk materials has played and will continue to play an instrumental role in developing strategies in the search for highly efficient thermoelectric materials, it should be kept in mind that these expressions are derived by using a set of approximations. Those related to the present discussion are given below.

1. Bulk density of states for electrons and holes. Expressions such as (6) and (7) are derived by assuming 3D parabolic bands. Quantum structures to be discussed later have a drastically different density of states and expressions (6) and (7) will change correspondingly.

2. Local equilibrium approximation. Expressions for the transport coefficients, equations (4) and (5), are derived by assuming that electrons deviate only slightly from their equilibrium distributions. This is valid only when the characteristic length along the transport direction is much longer than the electron mean free path. This assumption will not be valid for transport at the interfaces and for carrier transport in the direction perpendicular to very thin films. In addition, the electrons and phonons are typically assumed to be in thermal equilibrium. This assumption is not necessarily true, as in the well known hot electron effect in semiconductor electronics.

3. Isotropic relaxation time for both electrons and phonons. Many low-dimensional structures, such as superlattices, are highly anisotropic. Expressions such as equation (9) for the thermal conductivity are no longer correct.

Much of the development in low-dimensional structures can be attributed to relaxing one or several of these approximations. This allows for more independent control of S, σ, or k, as will be seen in the following discussion.

Low-dimensional thermoelectric materials

Low-dimensional materials, such as quantum wells, superlattices, quantum wires, and quantum dots offer new ways to manipulate the electron and phonon properties of a given material. In the regime where quantum effects are dominant, the energy spectra of electrons and phonons can be controlled through altering the size of the structures, leading to new ways to increase ZT. In this regime, the low-dimensional structures can be considered to be new materials, despite the fact that they are made of the same atomic structures as their parent materials. Each set of size parameters provides a 'new' material that can be examined, to a certain extent, both theoretically and experimentally, in terms of its thermoelectric properties. Thus, searching for high ZT systems in low-dimensional structures can be regarded as the equivalent of synthesising many different bulk materials and measuring their thermoelectric properties. Because the constituent parent materials of low-dimensional

structures are typically simple materials with well known properties, the low-dimensional structures are amenable to a certain degree of analysis, prediction and optimisation. In contrast, theoretical predictions for bulk materials properties are often difficult[23] and the investigation of each new material presents a different set of experimental and theoretical challenges. When quantum size effects are not dominant, it is still possible to utilise classical size effects to alter the transport processes, as for example the exploitation of boundaries to scatter phonons more effectively than electrons. Investigations over the past decade on low-dimensional structures have exploited both quantum and classical size effects for electrons and phonons. The focus of discussion here is along three directions. One is for electron transport parallel to the plane of thin films or along the axis of nanowires. Another is for the electron transport perpendicular to the film plane. The third emphasises phonon transport. Although no devices based on low-dimensional structures are close to commercialisation, research on low-dimensional thermoelectricity has been stimulating to recent developments in thermoelectrics research, and new research groups worldwide are now starting to bring new ideas to the field based on nanostructures.

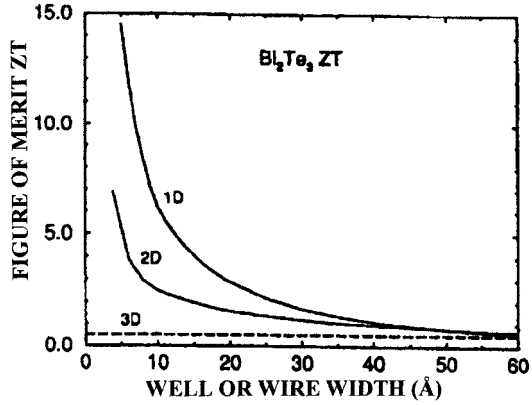

3 Calculated dependence of non-dimensional figure of merit *ZT* (within quantum well or within quantum wire) on well or wire width for Bi_2Te_3-like material at optimum doping concentration for transport in highest mobility direction: also shown is *ZT* for bulk (3D) Bi_2Te_3 calculated using corresponding 3D model[6,25]

Electron band gap engineered materials: transport parallel to film plane or nanowire axis

The development of band gap engineering in quantum structures for thermoelectric applications started with the modelling of single quantum wells[6] and soon moved on to the consideration of superlattices.[21] It was soon recognised that quantum wires would offer more quantum confinement and therefore would have advantages over quantum wells for thermoelectric applications,[24,25] as shown in Fig. 3. In due course, researchers also began to consider the benefits of quantum dot systems for thermoelectric applications. The key idea is to use quantum size effects to increase the electron density of states at the Fermi level and in this way to optimise the power factor. Further benefits to thermoelectric performance can be realised by exploiting boundary scattering to reduce the thermal conductivity preferentially, without much loss to the electrical conductivity.

Quantum wells and superlattices

The most elementary generic calculations,[6,24,25] and also more sophisticated calculations on specific materials,[26] both predict enhanced thermoelectric performance within the quantum wells of multiwell superlattices relative to bulk materials of the same stoichiometry. To show proof of principle experimentally, special superlattices were designed by the Dresselhaus group and fabricated by the Harman group at MIT Lincoln lab for PbTe based superlattices[27] and by the Wang group at UCLA to make Si/Ge superlattices.[28,29] The first proof of principles experiment to confirm the enhancement of *ZT* within a quantum well was reported for n-type PbTe quantum wells within $PbTe/Eu_xPb_{1-x}Te$ superlattices.[27] The results showed that the power factor within the PbTe quantum well could be increased by a factor of 4, and that the model calculations were in good agreement with the experimental observations. Soon thereafter, it was shown that an enhanced thermoelectric figure of merit could also be observed for p-type PbTe quantum wells,[30,31] which is, of course, an important consideration for thermoelectric devices, which depend on having both n-type and p-type legs.

These modelling calculations and experimental data are based on the consideration of transport inside the quantum wells only, and thus the reported *ZT* values are referred to as $(ZT)_{2D}$. Theoretical modelling pointed out that when the barrier regions of the superlattices are also considered, the overall gain in *ZT* of the whole structure is considerably reduced[32,33] because the barriers do not contribute to the electrical transport, but do contribute to the reverse heat conduction. In the limit that the barrier is thin, it was also suggested that tunnelling between quantum wells reduces the *ZT* enhancement inside an individual quantum well. How to address this issue is very important for the utilisation of quantum size effects on the electron transport along the film plane. One possible approach, suggested by the Dresselhaus group, is to use both the quantum wells and barriers for thermoelectric transport along the film plane.[34] For example, by proper choice of the widths of the quantum wells and barriers for GaAs/AlAs superlattices, the carriers in the Γ-point and L-point valleys contribute to transport in the GaAs regions, while the X-point valleys can contribute to transport in the AlAs regions.[35] Furthermore, for a given superlattice system, such as Si/Ge superlattices and their alloys,[36] model calculations can be used to optimise the superlattice geometry to achieve the maximum *ZT* of the whole superlattice structure. Although there are limited experimental data suggesting this possibility, more experimental efforts are needed to demonstrate the effectiveness of this carrier pocket engineering approach.

The theoretical work has inspired experimental studies of thermoelectric effects in superlattices. The past few years have seen steady improvements in the

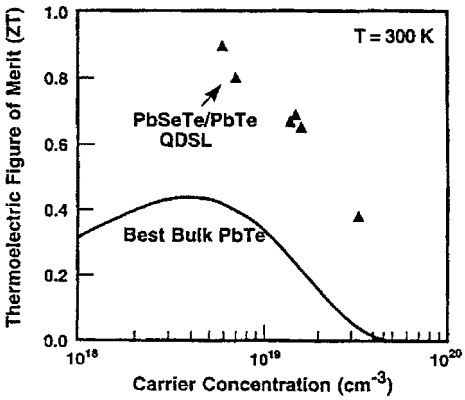

4 Thermoelectric non-dimensional figure of merit versus carrier concentration for high quality bulk PbTe material in comparison to much higher *ZT* for PbSeTe/PbTe quantum dot superlattice structure at 300 K[7] (courtesy T. Harman)

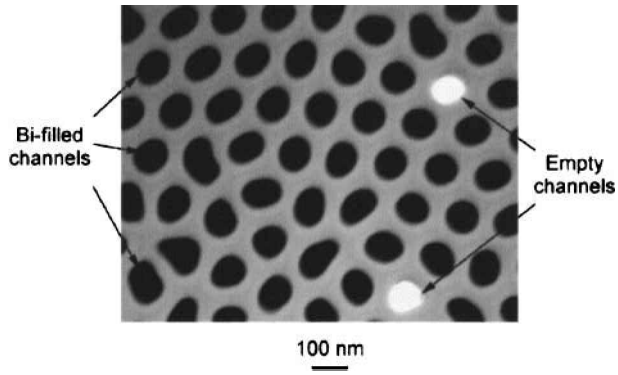

5 Cross-sectional view of Bi nanowires in cylindrical channels of 65 nm average diameter within anodic alumina template, shown as transmission electron microscope (TEM) image: template has been mostly filled with Bi, and TEM image was taken after top and bottom sides of sample had been ion milled with 6 kV Ar ions[44,48]

thermoelectric performance of specific superlattices. For example, experimental thermoelectric data from Harman's group demonstrated that for PbTe/Te superlattices, obtained by the addition of a few nanometres of Te above the PbTe layer before the barrier layer is added, the ZT increased from 0·37 to 0·52 at room temperature and this increase in ZT was associated with the formation of a quantum dot structure at the interface.[31] The Harman group further discovered experimentally that quantum dot superlattices based on PbTe/PbSeTe have an even higher ZT. For example, PbSeTe/PbTe quantum dot superlattices show a large enhancement in the Seebeck coefficient relative to bulk PbTe samples with the same carrier concentration.[7] At this stage, detailed mechanisms for the reported Seebeck coefficient enhancements in these quantum dot superlattices are not clear. Among the speculations are both quantum confinement effects and a more favourable scattering mechanism associated with quantum dots. Furthermore, an estimation of ZT for such quantum dot superlattices, based on the phonon thermal conductivity of equivalent alloys that are considered by the authors as conservative, yields a room temperature value of 0·9, which is more than a factor of 2 greater than has been achieved with the best bulk PbTe material (*see* Fig. 4). Efforts are presently underway by several groups worldwide to obtain reliable measurements of the in-plane thermal conductivity of small superlattice samples.[37–41] The growth by molecular beam expitaxy of PbTe based superlattices and quantum dot superlattices can be relatively fast, making it feasible to grow very thick superlattices (50–100 μm total thickness) for simple device testing.[42]

Quantum wires

General theoretical considerations suggest that, because of their increased quantum confinement effects, 1D quantum wires could have an even larger enhancement in ZT[24,43] than 2D quantum wells (*see* Fig. 3). To fabricate controlled arrays of quantum wires, anodic alumina (Al_2O_3) templates have been developed and these templates can be made to have regular triangular arrays of porous nanoscale channels from 7 to 100 nm in diameter and 50 μm in length with packing densities of 10^{10} channels cm^{-2} (Refs. 44, 45). These pores within the channels can then be filled with promising thermoelectric materials, such as Bi or $Bi_{1-x}Sb_x$ alloys. Because of the low effective masses and large anisotropy of the constant energy surfaces of these materials, quantum confinement effects at 77 K are predicted for wire diameters as large as 50 nm,[46] as discussed further below. These effects have been verified experimentally by transport measurements.[44,47]

Figure 5 shows an example of an anodised alumina template which is filled with Bi using the pressure injection method.[48] One important advantage of these Bi nanowires is their crystal properties which can be seen in the X-ray and electron diffraction patterns shown in Fig. 6 for an array of Bi nanowires 52 nm in average diameter, indicating that each wire has a similar crystal orientation along the nanowire axis. This is verified in Fig. 6 by comparison of the X-ray diffraction pattern with the corresponding electron diffraction pattern for a typical nanowire, showing a unidirectional orientation of the nanowires along the wire axes. In principle, the crystalline orientation can be controlled, but thus far the preferred growth direction for a given growth method has dominated the nanowire crystalline orientation. As a result of the high crystallinity of these nanowires, high carrier mobility and long mean free paths are achievable, which is of direct benefit for thermoelectric applications.

In addition to pressure injection, physical vapour deposition[49] has also been used to fill the templates and to make Bi nanowires with single crystal properties, having the same crystal structure and lattice constants as bulk Bi. Electrodeposition is very attractive for filling the pores of an alumina template, because of the ease in making good electrical contacts. The flexibility of the electrodeposition approach has allowed nanowire arrays of Bi, $CoSb_3$, and Bi_2Te_3 to be produced. The nanowire arrays thus far produced by electrodeposition are polycrystalline and are therefore expected to have lower carrier mobilities than

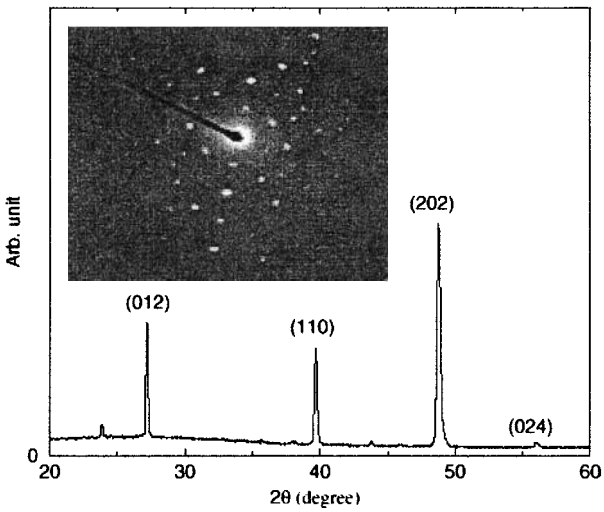

6 X-ray diffraction pattern for anodic alumina/Bi nanowire composites (average wire diameter of Bi nanowires is about 52 nm) and selected area electron diffraction pattern (inset) taken from same sample: these two experimental results indicate that Bi nanowires are highly crystalline and possess strongly preferred growth orientation[44,45]

the arrays prepared by filling from the vapour phase or by pressure injection.

Bismuth has a highly anisotropic band structure with some very small effective mass tensor components ($\sim 10^{-2}$ free electron masses), and high mobility carriers making it a very attractive thermoelectric material, except that in bulk form, Bi is a semimetal with equal concentrations of electrons and holes, thus leading to a nearly complete cancellation between the positive and negative contributions to the Seebeck coefficient. However, for Bi as a quantum well or a quantum wire, the band edge for the lowest subband in the conduction band rises above that for the highest subband in the valence band (*see* Fig. 7) thereby leading to a semimetal–semiconductor transition. This is predicted to occur at a wire diameter of 49 nm for Bi nanowires oriented along the favoured growth direction. Bismuth nanowires are of interest for thermoelectric applications when in the semiconducting regime, under heavy doping conditions.

Temperature dependent resistance measurements (*see* Fig. 8*a*) in conjunction with model calculations (*see* Fig. 8*b*) show that these bismuth nanowires are converted from a semimetal into a semiconductor due to quantum size effects.[50] This is seen by the monotonic temperature dependence of the resistance in the semiconducting phase for wire diameters below 48 nm and the non-monotonic behaviour with temperature for wires with diameters larger than 70 nm, above which the wires are in the semimetallic regimes, in agreement with theoretical predictions (Fig. 8*b*). The non-monotonic dependency of resistance on the nanowire diameter is due to the extrinsic carriers contributed by uncontrollable impurities, which becomes more important as band gap increases. So far, there exists no conclusive experimental data showing an enhanced power factor in Bi nanowire arrays, due to difficulties in measuring the absolute value of

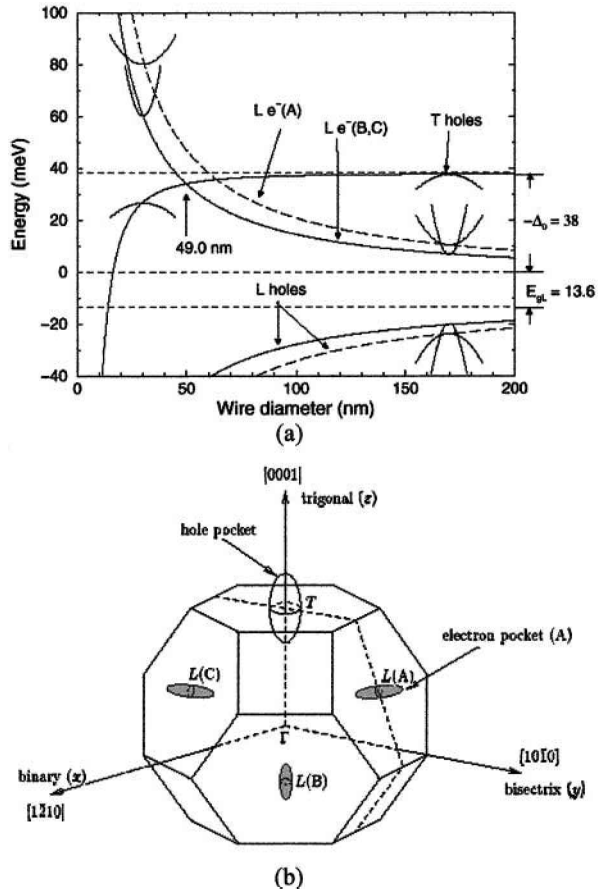

a subband structure at 77 K of Bi quantum wires oriented along [01$\bar{1}$2] growth direction, showing energies of highest subbands for T-point hole carrier pocket, L-point electron pockets (A, B and C) as well as L-point holes, which are indicated in Brillouin zone shown on right (zero energy refers to conduction band edge in bulk Bi): as wire diameter decreases, conduction subbands move up in energy, while valence subbands move down; at $d_c = 49{\cdot}0$ nm, lowest conduction subband edge formed by L(B,C) electrons crosses highest T-point valence subband edge, and semimetal–semiconductor transition occurs (Δ_0 is band overlap and E_{gL} is L-point band gap);[45] *b* Fermi surfaces of Bi, shown in relation to Brillouin zone corresponding to fifth-band hole pocket about T-point and three sixth-band L-point electron pockets labelled A, B, and C: mirror plane symmetry of bulk bismuth structure results in crystallographic equivalence of L-point carrier pockets B and C; however, L-point carrier pocket A is not equivalent crystallographically to carrier pockets B or C

7 Diameter dependence of band edges for Bi nanowires: 3D Brillouin zone in *b* shows important band edges participating in semimetal–semiconductor transition

the resistance of both nanowire arrays and of single nanowires. These difficulties arise from problems with making good ohmic contacts to all the nanowires of a nanowire array and with the oxidation of the individual nanowires, when they are removed from their templates.

The $Bi_{1-x}Sb_x$ alloy system is interesting as a method for obtaining a low-dimensional p-type semiconductor with very low effective masses and high mobility carriers, which is important because thermoelectric devices require both n-type and p-type legs. Since Sb is isoelectronic with Bi and has the same *A*15 crystal structure as Bi, bulk $Bi_{1-x}Sb_x$ alloys

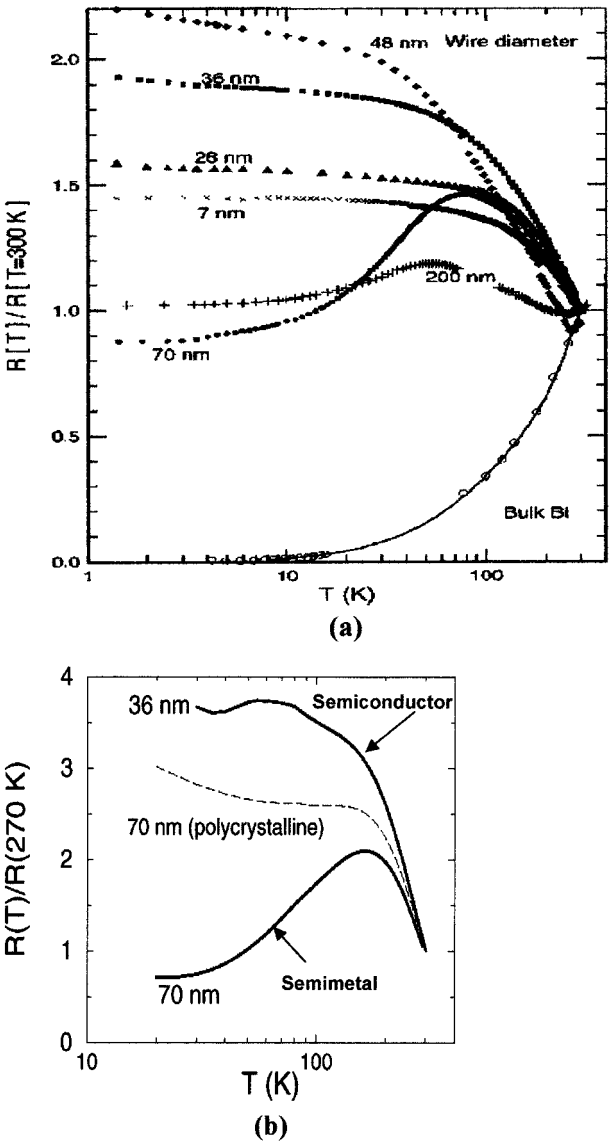

a experimental temperature dependence of normalised resistance for Bi nanowire arrays of various wire diameters prepared by vapour deposition method, in comparison with corresponding data for bulk Bi: measurement of resistance was made while Bi nanowires were in their alumina templates using two-probe measurement technique;[49] *b* calculated temperature dependence of resistance for Bi nanowires of 36 and 70 nm, using semiclassical transport model[45]

8 Temperature dependence of resistance measurements for Bi nanowires

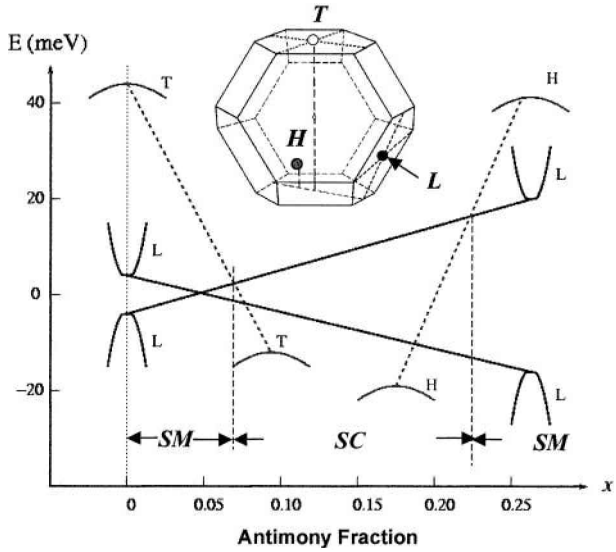

SM = regions where alloy is semimetal; SC = region where alloy is semiconductor

9 Schematic diagram for energy bands near Fermi level for $Bi_{1-x}Sb_x$ bulk alloys as function of x at low T (″ 77 K):[51] when highest valence band is at L-point, direct gap semiconductor results; for x values where highest valence states are at T or H, indirect semiconductor is obtained

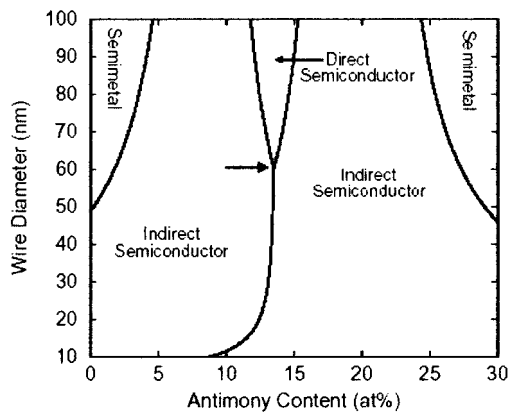

10 Phase diagram of electronic band structure of $Bi_{1-x}Sb_x$ nanowires:[52] bold arrow in centre indicates condition where 10 hole pockets (about T-point, 3 L-points and 6 H-points in Brillouin zone) coalesce in energy

provide a high mobility material, but with electronic properties that can be varied considerably as the Sb concentration is varied (*see* Fig. 9). Of particular interest for thermoelectric applications is the low Sb concentration range (below $x = 0{\cdot}07$) where the bulk material is semimetallic, the regions for $0{\cdot}07 < x < 0{\cdot}09$ and $0{\cdot}16 < x < 0{\cdot}22$ where bulk $Bi_{1-x}Sb_x$ is an indirect gap semiconductor and finally the region $0{\cdot}09 < x < 0{\cdot}16$ where bulk $Bi_{1-x}Sb_x$ is a direct gap semiconductor.[51] Calculations for the electronic structure for $Bi_{1-x}Sb_x$ nanowires (*see* Fig. 10)[52] show that variation of the wire diameter leads to another important degree of freedom in the control of the electronic structure, showing regions where, depending on the nanowire diameter and Sb alloy concentration, the wires are predicted to be semimetallic, a direct gap semiconductor, or an indirect gap semiconductor. The calculations of Fig. 10 show how variation of the nanowire diameter can be used to change the electronic structure quite dramatically with no basic change occurring in the crystal structures. Of particular interest in this diagram for the $Bi_{1-x}Sb_x$ nanowires is the point at $x = 0{\cdot}13$, and a wire diameter of 60 nm, where the L-point, T-point and H-point hole subband edges are all degenerate with one another, leading to a very large density of hole states. Such a system, where all 10 hole subband edges are degenerate in energy, is predicted to exhibit an enhanced Seebeck coefficient and an increased ZT.[52,53] The feasibility of observing interesting transport properties in $Bi_{1-x}Sb_x$ nanowires has been demonstrated by showing that the high degree of

crystallinity of the Bi nanowires is preserved upon Sb alloying as is the high carrier mobility.

Thus far, progress in the fabrication and measurement of the thermoelectric performance of test samples is most advanced for 2D systems where superior performance has already been demonstrated. The excellent ZT_{3D} for these superlattices is attributed to the presence of quantum dot structures at the nanoscale,[7] whose behaviour is not yet understood in detail, nor has the structure yet been optimised for thermoelectric performance. The 1D quantum wires have in contrast been modelled in detail, though materials problems involving surface oxidation and with the formation of good individual contacts to the nanowires have slowed the experimental evaluation and optimisation of the thermoelectric performance of the quantum wires. It is thus expected that further emphasis will be given to materials science issues, before the construction of reliable quantum wire thermoelectric devices will be seriously undertaken.

Electron transport perpendicular to film plane

Most of the effort so far has been focused on thin films and superlattices. There are two lines of consideration for electron transport perpendicular to the thin film plane: (i) control of the density of electron states using quantum size effects, and (ii) energy filtering through thermionic transport. Two theoretical papers considered quantum size effects on thermoelectric properties for electron transport perpendicular to the superlattice plane.[54,55] A slight increase in ZT for Si/SiGe superlattices made of extremely thin layers ($\sim$5 Å) is predicted.[54] Radtke *et al.*[55] studied $Hg_xCd_{1-x}Te$ superlattices, and their calculation shows that a 20% increase in power factor is possible in narrow-well narrow-barrier superlattice systems, but suggested that the gain in ZT will most likely come from a thermal conductivity reduction rather than from a power factor increase. So far, there seems to be no experimental effort aimed at pursuing a power factor increase due to quantum size effects for transport perpendicular to superlattice planes.

In the limit that the quantum size effect is not important, for this case, there is still a possibility for increasing ZT. It was proposed that the energy barriers at the junctions of different materials be used as an energy filter to increase the thermoelectric energy conversion efficiency.[8] Electron transport over such barriers is described by thermionic emission theory. In a theoretical paper, Mahan[56] considered the cooling power of vacuum based thermionic coolers, which are based on the same principle as vacuum based thermionic power generators. His calculation showed that vacuum based thermionic coolers will not be able to run at room temperature because of the large work function of known materials and because of space charge effects. Shakouri and Bowers[9] suggested that this could be circumvented using double heterojunction structures. The barrier height between two materials can be precisely tailored in theory as well as in practice for certain materials systems. Another advantage of this approach is that Joule heating is mostly rejected at the hot side due to the ballistic transport. Based on a simplified model, Shakouri and Bowers predicted that solid state thermionic coolers have a larger cooling power than that of thermoelectric devices. Mahan and co-workers[57,58] followed up with a thermionic cooling and power generation model for multiple layer structures. In this case, the advantage of the non-uniform heat generation inside a double heterojunction structure[9] due to the ballistic electron transport is lost. Their initial calculation[57,58] suggests that multilayer thermionic coolers can have a high efficiency. Yet in another paper, Vining and Mahan[59] compared the equivalent B factor that determines the ZT for thermionic multiple layer structures and similar thermoelectric multiple layer structures and found that the B factor of thermionic structures is not larger than that for thermoelectric structures. Their conclusion is that the thermal conductivity reduction[11,12] will be the major benefit of multiple layer structures, which is consistent with the studies carried out by the Ehrenreich group.[55] In addition to an all solid state cooling strategy, vacuum thermionic refrigeration based on resonant tunnelling through triangular wells and small spatial gaps in the vacuum has been proposed recently.[60,61] Theoretical calculations predict operation at room temperature and below, with a cooling power density of 100 W cm^{-2}. No net cooling based on such vacuum thermionic coolers has been reported experimentally.

Theoretically, the modelling of electron transport perpendicular to the confinement direction is considerably more difficult compared to that along the film plane, because the film thickness may be comparable to several characteristic lengths of the charge carriers, including the wavelength and the mean free path. Thus far, quantum based models, which consider the electrons as totally coherent, and thermionic emission models, which consider the electrons as totally incoherent, have been constructed. But there is no theory so far for the overlapping region. In addition, there are also thermoelectric effects inside the film, which may be coupled with thermionic effects at the interface to yield a total ZT of the structure. There have been a few studies that treat both effects and phonon size effects by Zeng and Chen.[62–64] Their modelling suggests that when the film is very thin, energy conversion is dominated by the thermionic emission and when the film is thick, thermoelectric transport governs the energy conversion efficiency. In the intermediate film thickness range, both effects contribute to the final ZT. Their work also suggests that the thermal conductivity reduction will contribute more to the ZT enhancement compared to the thermionic emission, ZT which is consistent with previous studies that inferred the importance of the thermal conductivity reduction based on experimental results.[55,59]

Experimentally, Shakouri and co-workers have fabricated thin film thermoelectric coolers based on single heterojunction structures[65] and superlattice structures[66–70] based on InP and Si/Ge superlattices. The maximum temperature rise measured on a single element device is 12 K at a 200°C substrate temperature from Si/Ge superlattices.[70] Mahan[10] pursued metal–semiconductor superlattice structures for cooling. No cooling effect has yet been reported from such structures. It should be emphasised that testing

a single device is very difficult and involves many forms of losses that may degrade the device performance. Thus, these devices may have better performance if successfully developed as arrays, rather than as individual devices. So far, there are no systematic experimental investigations on whether the observed cooling is due to thermionic or thermoelectric mechanisms, or both. Field emission coolers based on GaAs are also being investigated, but no cooling effect has been observed so far.[71]

Engineering phonon transport

Phonon transport in low-dimensional structures is also affected by size effects and can be utilised to increase ZT. Size effects in the thermal conductivity are a well known phenomenon that is important at low temperatures for bulk materials.[72] Several studies of the thermal conductivity of thin films were carried out in the 1970s and 1980s, mostly for polycrystalline metallic or semiconductor thin films. The first experiment on superlattices was performed by Yao[37] for the thermal conductivity along the film plane. He observed that the thermal conductivity of the superlattices investigated was higher than that for their compositionally equivalent alloys. One can easily infer that the reported values are also significantly lower than the values calculated from bulk properties according to the Fourier theory. The first experiment in the cross-plane direction was reported by Chen *et al.*[38] They measured the thermal conductivity of a semiconductor laser structure, which contained short period superlattices, in both directions and observed a factor of 10 reduction of k in the cross-plane direction compared to predictions by the Fourier theory. The reduction in the in-plane direction is smaller but also significant. In a review paper, Tien and Chen[73] suggested that the new spectrum in superlattices can potentially lead to super thermal insulators. The studies by Yao[37] and Chen and co-workers[38,39] were mainly geared towards thermal management applications for semiconductor lasers.[74] Venkatasubramanian proposed to use the potentially low cross-plane thermal conductivity of superlattices for thermoelectric devices.[11,75] The idea is to use the phonon reflection at interfaces to reduce the thermal conductivity, while maintaining the electron transmission at the interfaces by combining materials with small or, ideally, zero band-edge offset. Such structures are called electron-transmitting phonon-blocking structures. This strategy on the Bi_2Te_3/Sb_2Te_3 system seems to have led to a significant increase of ZT[11,76] as indicated in Fig. 2. As a word of caution, because the characterisation of ZT is extremely difficult in this direction, the values should be supported by more research, preferably by different groups.

Extensive experimental data on the thermal conductivity of various superlatttices, including Bi_2Te_3/Sb_2Te_3,[75,77,78] GaAs/AlAs,[37–39,79,80] Si/Ge,[40,81–83] InAs/AlSb,[84] InP/InGaAs,[85] $CoSb_3/IrSb_3$,[86] and PbTe based superlattice[41] have been reported in recent years. Most of these measurements are in the cross-plane direction,[75,81–86] using the 3ω method[87] or the optical pump-and-probe method.[80] Measurements along the film plane direction relied heavily on the removal of the substrate.[37–39,83] Very few studies have reported thermal conductivity in both the in-plane and cross-plane directions.[38,40] All these experiments confirmed that the thermal conductivities of the superlattices in both directions are significantly lower than the predictions based on the Fourier law and the properties of their bulk parent materials. In the cross-plane direction, the thermal conductivity values can definitely be reduced below that of their corresponding alloys.[12,81] In the in-plane direction, the reduction is generally above or comparable to that of their equivalent alloys,[40] although a few experimental data indicate that k values lower than those of the corresponding alloys are possible.[11]

A few groups have developed theoretical explanations for the thermal conductivity of superlattices, for both in-plane and cross-plane directions. Two schools of thought are apparent from the literature. One starts from the phonon spectrum calculation and attributes the thermal conductivity reduction to changes in the group velocity, density of states, and scattering mechanics.[88–93] The other approach starts from the simple picture of interface reflection and treats phonon transport in terms of particles.[94–97] The former assumes that phonons are totally coherent and the latter treats phonons in each layer as totally incoherent. The coherent phonon picture is accurate if the interfaces and internal scattering do not destroy the coherence of the phonons. Compared to the coherent picture, the particle approach does not treat the following mechanisms correctly: (i) phonon interference, which gives minigaps in the superlattice phonon spectrum, (ii) phonon tunnelling, which occurs for very thin layers above the critical angle for total internal reflection of phonons, and (iii) long wavelength phonons, which do not 'see' the existence of the interfaces. These three factors, however, do not seem to be dominant in the observed thermal conductivity behaviour of superlattices. This is because heat conduction involves the contribution from all allowable phonons covering the entire phonon frequency range. Minigaps created by interference effects cover only a small fraction of the total thermal energy. Tunnelling is important only when each layer is only 1–3 monolayers thick due to the small phonon wavelength. In addition, the diffuse interface scattering occurring at most interfaces, which seems to be a very important factor, destroys the phonon coherence. Comparison of lattice dynamics,[92] acoustic wave propagation,[98] and Boltzmann equation[94,96,97] simulations with experimental data, by Chen and co-workers, leads to the conclusion that the major reason for the observed thermal conductivity reduction in the cross-plane direction is the phonon reflection, particularly the total internal reflection.[12] Although phonon confinement due to the spectral mismatch can potentially contribute significantly to the thermal conductivity reduction, it is likely that many phonons leak out due to inelastic scattering. For both the in-plane and the cross-plane directions, diffuse interface scattering of phonons seems to play a crucial role. As an example, in Fig. 11*a* the simulated thermal conductivity reduction in Si/Ge superlattices in both the in-plane and the cross-plane directions based on lattice dynamics modelling of the phonon

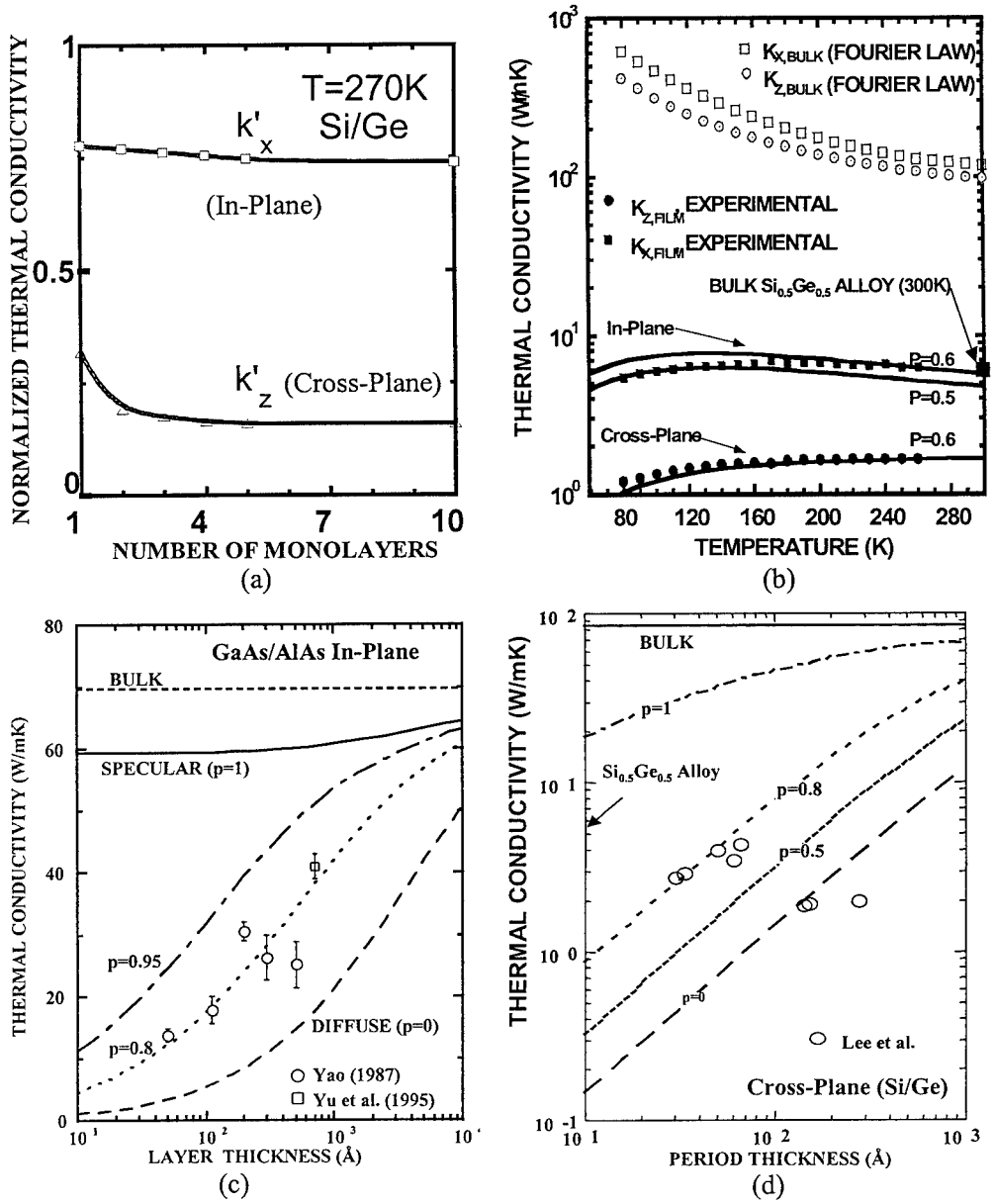

a lattice dynamics simulation of thermal conductivity normalised to bulk values;[92] *b* temperature dependence of thermal conductivity of Si/Ge (20/20 Å) superlattice along (subscript x) and perpendicular (subscript z) to film plane;[40] *c* thickness dependence of thermal conductivity of GaAs/AlAs superlattices along film plane (GaAs and AlAs layers are of equal layer thickness);[94] *d* period thickness dependence of thermal conductivity of Si/Ge superlattices in cross-plane direction[97] (also plotted in *b–d* are fittings based on solutions of Boltzmann equations with *p* representing fraction of specularly scattered phonons at interface, and values calculated based on Fourier law and measured bulk thermal conductivities of Si and Ge)

11 Results indicating crucial role of diffuse interface scattering of phonons

spectrum in superlattices[92] is shown in comparison to experimental results (Fig. 11*b*–11*d*)[40] on a Si/Ge superlattice. The simulation based on the phonon group velocity reduction leads to only a small reduction in k in the in-plane direction, while the cross-plane direction shows a relatively large drop (Fig. 11*a*). The lattice dynamics models imply perfect interfaces and thus no diffuse interface scattering. Experimentally, the thermal conductivity reductions in both directions are much larger, as shown in Fig. 11*b*. In addition, the lattice dynamics simulation leads to a thermal conductivity that first decreases with increasing superlattice period thickness and then approaches a constant that is significantly lower than that of its corresponding bulk values. Such behaviour is contrary to most experimental observations on GaAs/AlAs superlattices and Si/Ge superlattices, as shown in Fig. 11*c* and 11*d*,[94,97] except in the very thin layer region where experimental data on Bi_2Te_3/Sb_2Te_3 superlattices indeed show a recovery trend with decreasing period thickness.[11] Acoustic wave simulation suggests that the recovery in the thermal conductivity at the very thin period limit is due to the tunnelling of phonons from one layer into another for incidence above the critical angle.[98] In reality, however, there also exists the possibility that such a recovery is due to interface mixing that creates alloys rather than superlattices. In the thicker period regime, the Boltzmann equation based modelling that treats phonons as particles experiencing partially

specular and partially diffuse scattering at the interfaces, can lead to a reasonable fit to the experimental data, as shown in Fig. 11*b*–11*d*. The parameter p in Fig. 11*b*–11*d* represents the fraction of specularly scattered phonons at the interface and $(1-p)$ that of the diffuse scattering that may be caused by interface mixing and roughness, or anharmonic forces at the interface. The agreement between modelling and experimental results suggests that the phonon coherence length in superlattices is short and the loss of coherence is probably due to diffuse interface scattering.

To exhibit significant size effects, the phonon mean free path in the bulk material should be larger than the film thickness or other characteristic lengths of the structure. The estimation of the phonon mean free path, however, must be done carefully. Often, one tends to estimate the phonon mean free path Λ from the simple kinetic formula $k = Cv\Lambda/3$, using the specific heat and speed of sound in bulk materials. The mean free paths of phonons that actually carry the heat could be much longer, because: (i) optical phonons contribute to the specific heat but not much to thermal conductivity due to their small group velocity, and (ii) the acoustic phonon group velocity can be much smaller than the speed of sound due to dispersion effects. For example, a careful estimation of the phonon mean free path in silicon leads to 2500–3000 Å,[97,99] compared to the kinetic theory value of $\sim$400 Å. Because of this, some apparently low thermal conductivity materials, such as Bi_2Te_3/Sb_2Te_3 and $CoSb_3/IrSb_3$ superlattices, can actually be engineered to have lower values by exploring size effects. Another important point is that typically the thermal conductivity reduction in the cross-plane direction is larger than in the in-plane direction because interfaces impede the phonon transport more in the cross-plane direction than along the film plane, as is suggested by Fig. 11*b*. For polycrystalline materials this may not necessarily be true, because the columnar grain structures can actually cause a more significant reduction in the in-plane direction, as is observed in diamond thin films.[100] Other factors such as the dislocation orientation (occurring in threading dislocations) may also create more scattering in the in-plane direction, although there have been neither detailed theoretical nor experimental studies.

Existing experimental data have clearly shown that the thermal conductivity of superlattices can be made smaller than that of their corresponding alloys. Remember that alloying has been used in thermoelectric materials research as an effective way to reduce the lattice thermal conductivity. This raises the question of what is the minimum thermal conductivity of superlattices. Slack[101] proposed that the minimum thermal conductivity one can reach for a material is when the phonon mean free path in equation (9) is replaced by the wavelength. Later, Cahill *et al.*[102] further limited it to half the wavelength. The more fundamental question is whether low-dimensional structures are subject to the same limit or not. Chen[12] argued that the same minimum may not be applicable to low-dimensional materials which are highly anisotropic, because anistropy causes directional dependence of the relaxation time and of the group velocity. He proposed that the correct starting point should be from the following expression for the thermal conductivity

$$k_p = \frac{1}{4\pi}\int_0^{\omega_{max}} \left\{ \int_0^{2\pi} \sin^2\varphi \, d\varphi \left[\int_0^{\pi} C(\omega) v(\omega,\theta,\varphi) \times \Lambda(\omega,\theta,\varphi) \cos^2\theta \sin\theta \, d\theta \right] \right\} d\omega \quad . \; . \; . \; (10)$$

where θ and φ are the polar and azimuthal angles formed with the heat flux direction. The task of reducing the thermal conductivity is to reduce the value of the above integral. Low-dimensional structures offer several new ways to reduce the thermal conductivity integral in equation (10). First, the group velocity can be altered in nanostructures. The formation of standing waves in nanostructures means that the group velocity becomes smaller, thus reducing the thermal conductivity. In superlattices, the bulk acoustic phonons can be changed into optical phonons, thereby drastically reducing their group velocity. Second, it is possible to induce anisotropic scattering in low-dimensional structures. For example, interface reflection and transmission are highly angle dependent. Total internal reflection means that phonons above the critical angle will be reflected backwards. As another example, the optical phonons in two materials have totally different frequencies. It is likely that the scattering of optical phonons at the interface will be highly directional, i.e. the optical phonons will be preferentially scattered backwards. In the context of the phonon dispersion curve, this is called phonon confinement. The effects of total internal reflection and the phonon confinement on the thermal conductivity can also be interpreted as reducing the angle and frequency integration limits of equation (10), thus decreasing the thermal conductivity. Third, the specific heat of nanostructures can be changed by changing: (i) the density of states and (ii) the degrees of freedom of the atomic vibrations. Theoretical studies on superlattices, however, suggest that these changes are not strong, except at low temperatures.[103–105] Based on these arguments, Chen[12] suggested that low-dimensional structures may have a smaller minimum thermal conductivity. Figure 12 shows the experimental thermal conductivity of a Si/Ge superlattice compared to predictions based on the minimum theoretical thermal conductivity of bulk Si and Ge. The figure suggests the possibility of reaching values lower than that theoretically attainable in bulk materials.

Thus, it seems that the following strategies may be pursued to engineer the phonon transport in order to reduce the lattice thermal conductivity.

1. For transport along the interfaces, i.e. along the film plane and wire axis, the thermal conductivity can be reduced by creating diffuse interface scattering and reducing the interface separation distance. In addition to the naturally existing interface roughness due to the mixing of atoms at the interfaces, other possibilities are artificially corrugated interfaces, such as thin films grown on step-covered substrates, and quantum dot interfaces. In controlling the interface structures for phonon thermal conductivity reduction, the

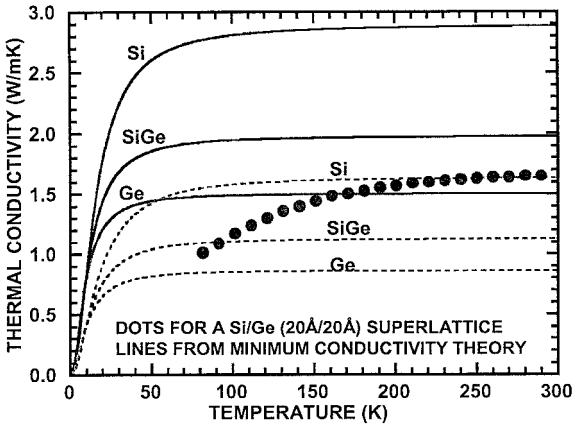

12 Comparison of measured thermal conductivity of highly dislocated Si/Ge superlattice with predictions of minimum thermal conductivity theory for bulk Si and Ge and their multilayer composite, latter is calculated based on Fourier theory:[12] solid and dashed lines are from minimum thermal conductivity theories by Slack[101] and Cahill *et al.*[102] respectively

interface effects on the electron transport must also be considered. It may, however, be possible to capitalise on the different wavelengths of electrons and phonons, such that phonons are scattered more diffusely at the interface than electrons, because the dominant phonon wavelength is typically shorter than the electron wavelength.

2. For transport perpendicular to the interfaces, increasing the phonon reflectivity is the key strategy for reducing the thermal conductivity. This could be realised by increasing the mismatch between the properties of the two constituents, such as the density, group velocity, specific heat, and the phonon spectrum between adjacent layers. The effects of interface roughness can be positive or negative, depending on whether the diffuse phonon scattering actually decreases or increases the phonon reflectivity at the interfaces. Experiments and modelling so far seem to indicate that diffuse scattering is more effective when the mismatch in the material properties is not large. Phonon confinement occurs due to the mismatch between the bulk phonon dispersion relations, and a large difference in the dispersion favours more phonon confinement. How much phonon confinement can be achieved, however, is an open question. Needless to say, however, in pursuing the phonon thermal conductivity reduction, the effects of interfaces on the electron transport must be considered. Past studies on electron transport, particularly in the development of vertical-cavity surface-emitting lasers (VCSELs), indeed suggest the possibility of much stronger reduction in the thermal conductivity than in the electrical conductivity. For example, digitally or continuously graded interfaces are often used to reduce the electrical resistivity of Bragg reflectors used for VCSELs,[106] while it is likely that such graded interfaces can create more phonon back reflection and thus a larger thermal conductivity reduction.[38]

3. Some long wavelength phonons may not 'see' the interfaces in structures, such as superlattices. The localisation of these phonons can further decrease the lattice thermal conductivity. Using aperiodic rather than periodic superlattices, or composite superlattices with different periodicities, may provide methods to localise some, if not all, of these long wavelength phonons.

4. Defects, particularly dislocations, can provide another vehicle to reduce the lattice thermal conductivity in low-dimensional systems. Clearly, whether all or some of these strategies will work for the improvement of the energy conversion efficiency will depend on their impacts on the electron/hole energy conversion capabilities. More studies of these effects should be done.

The phonon size effects in quantum wires and quantum dots are conceivably more significant than in thin films and superlattices due to their increased surface/interface area. Up to now, studies of the thermal conductivity of quantum wires have been scarce. There are a few experimental and theoretical studies on the thermal conductivity of quantum dot arrays and nanostructured porous media.[107,108] Theoretically, one can expect a larger thermal conductivity reduction in quantum wires compared to thin films.[109,110] The measurements of the thermal conductivity in quantum wires have been challenging. Recent measurements on the thermal conductivity of individual carbon nanotubes[111] provide a possible approach for related measurements on thermoelectric nanowires of interest. Nanowires for thermoelectrics, however, have very low k compared to carbon nanotubes, and this large difference in behaviour will create new challenges for measurements on nanowires of interest to thermoelectricity.

Bulk materials

The search for 'phonon–glass electron–crystal' bulk materials has now moved beyond the traditional Bi_2Te_3 based binary system. Several classes of bulk materials have been discovered or re-investigated as interesting for potential thermoelectric applications. Representative among them are skutterudites, clathrates, β-Zn_4Sb_3, half-Heusler intermetallic compounds, and complex chalcogenides. The phonon rattler concept developed by Slack has proven to be very effective in reducing the thermal conductivity of materials with open cages, such as skutterudites and clathrates. The highest ZT in filled skutterudites reached 1·4 at $\sim$600°C, as shown in Fig. 2. In this section, several promising bulk thermoelectric materials will be briefly reviewed.

Skutterudites

Existence and composition

In the early 1990s, a systematic search for advanced thermoelectric materials resulted in the 'rediscovery' of a family of attractive semiconducting materials with the skutterudite crystal structure.[112] For state of the art thermoelectric materials, such as PbTe and Bi_2Te_3 alloys, the number of isostructural compounds is limited and the possibilities to optimise their bulk properties for maximum performance at different temperatures of operation are also very limited. This is not the case for the skutterudite family of materials, where 11 binary compounds and many solid solutions and related phases are known to exist.[113] These

materials cover a large range of decomposition temperatures and band gaps, which offer the possibility to adjust the composition and doping level for a specific temperature range of application. An excellent in-depth review of skutterudites as novel thermoelectric materials was recently written by Uher.[114]

The unit cell of the skutterudite structure (cubic, space group *Im*3, prototype $CoAs_3$) contains square radicals $[As_4]^{4-}$. This anion, which is located in the centre of the smaller cube, is surrounded by 8 trivalent transition metal Co^{3+} cations. The unit cell consists of 8 of these smaller cubes, or octants, two of them empty, and six of them containing the anions $[As_4]^{4-}$ in the centre. This arrangement is necessary to maintain the stoichiometric ratio $Co^{3+} : [As_4]^{4-} = 4 : 3$. Taking into account one-half of the full 32 atom unit cell and its empty octant, one can represent the skutterudite formula as $\square T_4 Pn_{12}$, where $\square$ is the empty octant, T is the transition metal and Pn is the pnicogen atom. If considering a simple bonding scheme,[115] each transition metal contributes 9 electrons and each pnicogen contributes 3 electrons to the covalent bonding, for a valence electron count (VEC) total of 72 for each $\square T_4 Pn_{12}$ unit. The VEC is a useful number in determining the skutterudite compositions that are semiconducting. The valence electron count of 72 corresponds to a diamagnetic semiconductor for the skutterudite materials. Uher[114] gave a detailed discussion on the bonding scheme that favours the semiconducting behaviour. There are eleven $\square T_4 Pn_{12}$ binary skutterudites reported in the literature. The nine semiconducting compositions are formed with all nine possible combinations of T = Co, Rh, Ir and Pn = P, As, Sb. Two additional skutterudite phosphides were reported, NiP_3 and PdP_3. However, in these two compounds, the total VEC is 73, resulting in metallic behaviour.[116]

The existence of many ternary skutterudites has been determined. Nine ternary compounds have been reported in the literature, and at least 17 more have been discovered.[117] Ternary skutterudite compositions are derived from binary compounds by keeping a total VEC of 72. Using $\square Co_4 Sb_{12}$ ($CoSb_3$) as an example, substituting trivalent Co (Co^{3+}) by divalent Fe (Fe^{2+}) and tetravalent Pd (Pd^{4+}), results in $\square Fe_2 Pb_2 Sb_{12}$ ($Fe_{0.5} Pb_{0.5} Sb_3$). If instead, Sb is replaced by Sn and Te, then $\square Co_4 Sn_6 Te_6$ ($CoSn_{1.5} Te_{1.5}$) is obtained. If substitutions occur on both the transition metal and pnicogen sites, then $\square Fe_4 Sb_8 Te_4$ ($FeSb_2 Te$) is obtained.

A filled skutterudite structure is simply derived from the skutterudite structure by inserting one atom in each empty octant, as illustrated in Fig. 13. A large number of these compounds have been known for some time (*see* e.g. Refs. 116, 118–121), where the filling atom is typically a rare earth lanthanoid, though other compositions with actinoids Th and U,[121,122] as well as alkaline earths Ca, Sr and Ba[121,123] have also been reported. For a typical filled skutterudite composition, such as $LaFe_4 P_{12}$, the rare earth element contributes 3 electrons, but due to the divalent Fe (Fe^{2+}), the total VEC is only 71. This deficit results in metallic behaviour for most simple filled ternary compounds. Only $CeFe_4 P_{12}$, $UFe_4 P_{12}$ and $CeFe_4 As_{12}$ have been reported as semiconductors.

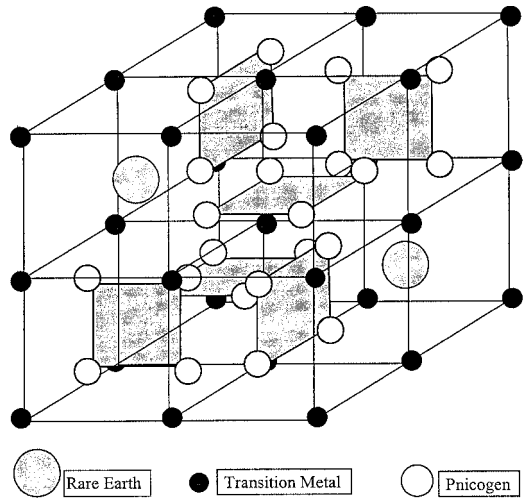

13 Schematic of filled skutterudite 34 atom unit cell of novel thermoelectric materials – each cell contains 8 transition metal atoms: Fe, Ru, Os, Co, Rh, Ir, Ni, Pd or Pt; 24 pnicogen atoms: P, As, Sb (substitution by S, Se or Te possible); 2 rare earth atoms filling vacant octants in skutterudite structure: La, Ce, Pr, Nd, Sm, Eu, Gd, Th and U

It should be noted, however, that even if a simple VEC scheme may be used to explain the various atomic composition permutations in skutterudites, the actual picture is certainly quite a bit more complicated, especially when trying to explain the transport properties of the more complex skutterudites, in view of some doping and compositional limitations. Much effort has been devoted in recent years to understanding the valence of transition metals and some rare earth filling atoms in ternary and filled skutterudites but results are somewhat inconclusive at this point.[114]

Transport properties

The transport properties of both n-type and p-type conductive binary skutterudite compounds, mostly antimonides and arsenides, have been thoroughly characterised in the past few years (*see* e.g. Refs. 124–126). Associated with a low hole effective mass, very high hole mobilities, low electrical resistivities and moderate Seebeck coefficients are obtained in p-type skutterudites (Fig. 14). Most of the samples shown in this figure were not nominally doped. They were grown using a gradient freeze technique from non-stoichiometric, Sb rich melts.[127] One should note that the room temperature mobility values of p-type skutterudites are very high (Fig. 14*a*), about 10 to 100 times higher than those for p-type Si and GaAs at similar carrier concentrations. $RhSb_3$ exhibits the greatest hole mobility, 8000 $cm^2 V^{-1} s^{-1}$ for a carrier concentration of $2{\cdot}5 \times 10^{18}$ cm^{-3}, which is about 70 times higher than p-type GaAs and still 5 times higher than n-type GaAs. For a comparable doping level, the carrier mobilities of n-type samples are about an order of magnitude lower than the values achieved on p-type samples. However, the much larger electron effective masses and Seebeck coefficients make n-type skutterudites promising candidates as well.

Unfortunately, the room temperature thermal conductivity of binary skutterudites (10–25 W $m^{-1} K^{-1}$)

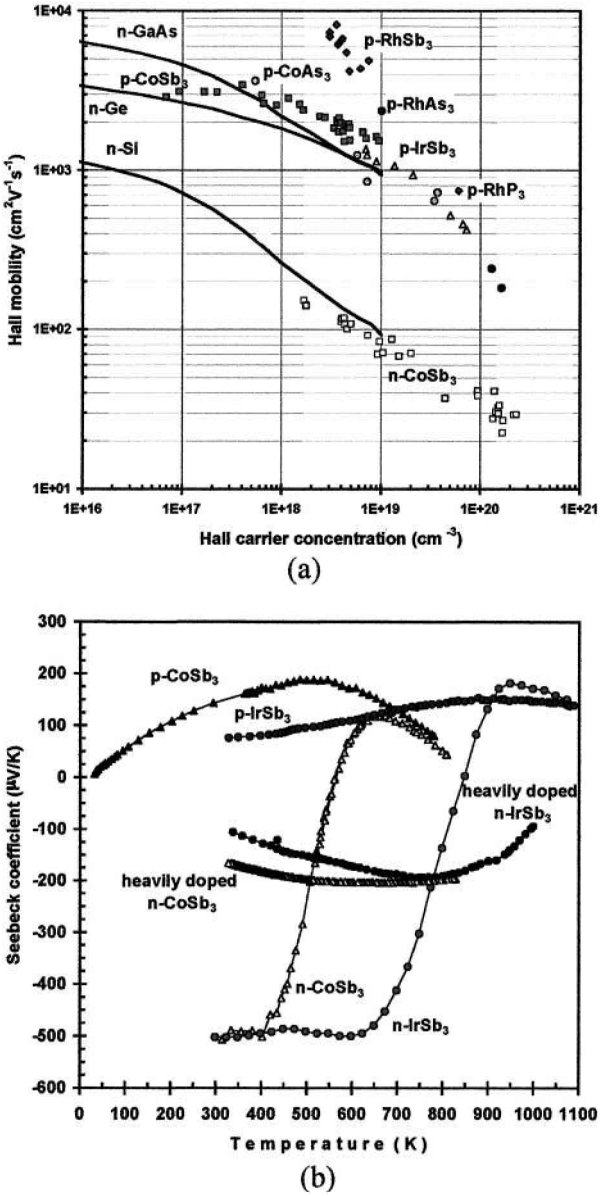

14 ***a*** **Hall mobility variation as function of carrier concentration and** ***b*** **Seebeck coefficient as function of temperature for binary skutterudite compounds: samples were not nominally doped[127]**

is too high to result in high ZT values. Substantial reductions in the lattice thermal conductivity must be obtained to achieve values comparable to those of state of the art thermoelectric materials (1–4 W m^{-1} K^{-1}). Several approaches to the reduction of the lattice thermal conductivity in skutterudites have been pursued: heavy doping, and formation of solid solutions and alloys, as well as the study of novel ternary and filled skutterudite compounds. All those approaches have resulted in skutterudite compositions with substantially lower thermal conductivity values. The room temperature lattice thermal conductivity and carrier concentration values of selected skutterudite compounds and alloys are reported in Table 1 for comparison. It is interesting to note that, compared to binary compounds, the lattice thermal conductivity values can be one order of magnitude lower in some ternary unfilled or filled compositions. Also, as shown in the table, high doping levels in n-type $CoSb_3$ result in a 70% reduction in lattice thermal conductivity, an effect comparable to that obtained by forming solid solutions. As a result, ZT values as high as 0·85 are obtained in the 850–900 K temperature range in heavily doped n-type $CoSb_3$,[128] as shown in Fig. 2.

These experimental results thus demonstrate that the skutterudite family of compounds and alloys offer extremely attractive possibilities for the search for high ZT materials. Skutterudites have excellent electrical transport properties and the thermal conductivities can be reduced by a factor of 20, down to nearly glassy characteristics. Since the work of Chasmar and Stratton,[129] it has been obvious that high ZT values require materials with a high mobility, high effective mass and low lattice thermal conductivity, where ideally one can separately optimise the power factor and minimise the thermal conductivity, or as summarised by Slack,[5] fabricate a PGEC. While the conceptual approach to high ZT has been known for over 40 years, much effort has been devoted into finding out if skutterudites could truly be such PGEC materials, that is conserving the excellent electrical properties of the binary compounds while reducing the thermal conductivity to values substantially lower than that of state of the art of Bi_2Te_3 alloys.

However, a number of experimental and theoretical results published in recent years on both ternary unfilled and filled skutterudite compounds indicate that their electronic band structure and transport properties are vastly different from the pure binary compounds.[130,131] For example, the study of such ternary compounds as $FeSb_2Te$, $Fe_{0.5}Ni_{0.5}Sb_3$ and $Ru_{0.5}Pd_{0.5}Sb_3$ derived from high carrier mobility $CoSb_3$ and $RhSb_3$ shows that they are heavily doped semiconductors with carrier concentration values ranging from 1×10^{20} to 1×10^{21} cm^{-3}. Comparing these compounds to $CoSb_3$ at such high carrier concentrations, they are characterised by significantly lower carrier mobility, and lattice thermal conductivity values as much as 50 to 75% lower. Such low lattice thermal conductivity values are somewhat

Table 1 Room temperature conductivity type, carrier concentration N, and lattice thermal conductivity k_p of various skutterudite compounds and alloys, including filled compositions

Compound	Conductivity	N, cm^{-3}	k_p, W m^{-1} K^{-1}
CoP_3	p	3×10^{19}	23·7
$CoAs_3$	p	4×10^{18}	14·0
$CoSb_3$	p	9×10^{18}	10·3
$CoSb_3$	n	1×10^{21}	3·4
$CoP_{1.5}As_{1.5}$	p	5×10^{18}	3·8
$Co_{0.88}Ir_{0.12}Sb_3$	p	1×10^{19}	2·9
$FeSb_2Te$	p	5×10^{20}	2·3
$OsSb_2Te$	p	4×10^{18}	2·1
$RuGe_{0.2}Sb_2Te_{0.8}$	p	9×10^{19}	1·4
$Ru_{0.5}Pd_{0.5}Sb_3$	p	1×10^{20}	1·5
$IrSn_{1.5}Se_{1.5}$	p	3×10^{19}	2·7
$CeRu_4P_{12}$	p	1×10^{20}	8·0
$CeFe_4Sb_{12}$	p	3×10^{21}	1·6
$Nd_{0.7}Ru_2Co_2Sb_{12}$	p	2×10^{20}	1·8

surprising considering that the atomic mass and volume differences introduced by the substituting anion/cation are fairly small: Fe and Ni for Co, Ru and Pd for Rh, Te for Sb. A possible explanation given for the unusually high phonon scattering rate is that transition metal elements have mixed valence states and electrons are transferred between the different ions, thus scattering the phonons in this process.[132,133] This would be consistent with low carrier mobilities as well as with the experimental difficulties encountered in controlling their electrical properties since changes in carrier concentration are not easy to achieve because dopants can be compensated by small fluctuations in the overall valence of the transition metals.

Interestingly enough, the search for high ZT values in skutterudites has been most successful so far in compounds that do not share the exceptional carrier mobilities of the pure binary compounds, but rather have a combination of high degeneracy, unusually large Seebeck coefficient values and low lattice thermal conductivities: filled and partially filled skutterudites. A maximum ZT value of 1·4 has been achieved to date at a temperature of 875 K in $Ce_f Fe_{4-x} Co_x Sb_{12}$ and $La_f Fe_{4-x} Co_x Sb_{12}$, where $f<1$ and $0<x<4$.[134,135]

The initial appeal of introducing a filling atom into the skutterudite structure was to substantially reduce the lattice thermal conductivity of the original binary compound with minimal decrease in the carrier mobility, and thus to achieve a 'PGEC'. The heavy filling atom would 'rattle' within its octant 'cage' and thus scatter phonons quite effectively. Also because it is filling an empty octant, its contribution to the electrical transport would be minimal, though the increased phonon scattering rate should somewhat impact the carrier scattering rate (carrier–phonon interaction). However, it became rapidly clear that filled skutterudites are quite different from their binary relatives, and that their low lattice thermal conductivities result from a combination of effects, often quite difficult to separate from each other: rattling, carrier–phonon scattering (high doping levels), mixed valence of the transition metals, point defect scattering.

If comparing fully filled compositions and taking into account charge carrier concentration levels, however, it can be shown that the lattice thermal conductivity does indeed decrease significantly with increasing rattling amplitude of the filling atom, as shown in Fig. 15. The rattling amplitude is defined as the difference between the void filler covalent radius and the radius of the cage.[136] The rattling amplitude increases are the largest when going from the phosphides to the antimonides which have larger unit cells and cage sizes, and very little when going from Fe based to Ru based compositions.

The most recent research efforts on skutterudites have focused on improving ZT over a wide temperature range by attempting to conserve the excellent semiconducting behaviour of the unfilled binary skutterudites when introducing a 'compensating' atom for the addition of the 'filling' atom into the structure, and going back to a VEC of 72. However, preparing lightly doped extrinsic p-type and n-type compos-

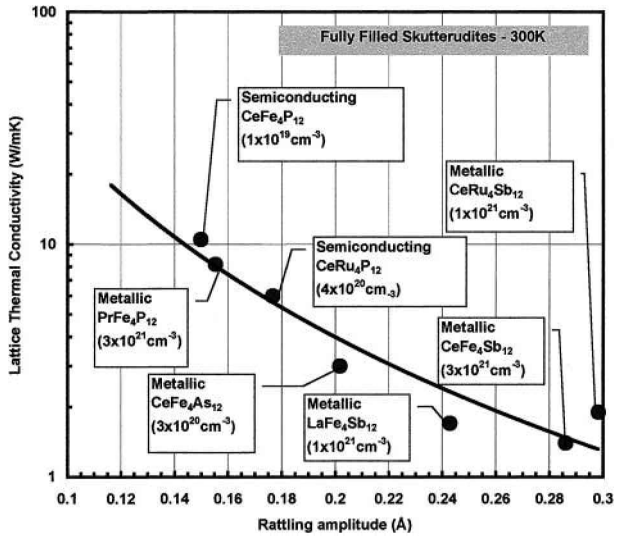

15 Room temperature lattice thermal conductivity as function of filling atom rattling amplitude for various fully filled and fully dense filled skutterudite compounds: carrier concentrations are also reported to account for additional charge carrier scattering of phonons

itions has proven quite challenging from a materials synthesis standpoint. Electron microprobe analysis of a series of $Ce_f Fe_{4-x} Co_x Sb_{12}$ compounds has demonstrated that the fraction of Ce filling f decreases with increasing substitution of Fe by Co. In addition to Co, substitution of Fe by Ni and Ru, and the substitution of Ru by Pd have also been investigated recently. The variations of the filling fraction f as a function of x are plotted in Fig. 16 for the four different ranges of compositions. The two solid lines represent the expected transition for Ni and Co from p-type to n-type (when the VEC reaches 72), taking into account both f and x variations. When Fe is totally replaced by Co, only a very small amount of Ce remains in the sample ($f=0{\cdot}07$). The chain dotted line was calculated based on a $CeFe_4Sb_{12}$–$Ce_{0{\cdot}065}Co_4Sb_{12}$ range of 'solid solution' compositions. $Ce_f Fe_{4-x} Ni_x Sb_{12}$ compositions with $x>1{\cdot}5$ have not yet been synthesised, but it is clear that at equivalent concentrations, Ni substitution results in less Ce filling than Co substitution. However, because Ni donates two electrons instead of only one for Co when replacing Fe, the decrease in carrier concentration and the corresponding change in properties with increasing x is much stronger for $Ce_f Fe_{4-x} Ni_x Sb_{12}$. One can see from these results that semiconducting compositions can be obtained for Co rich compositions. However, they typically show mixed conduction effects at room temperature.[117]

Recent theoretical studies on n-type filled skutterudites[137] and new experimental materials preparation approaches through high pressure, high temperature synthesis or the use of thin interdiffusing layers[138,139] may eventually allow for the characterisation of 'optimised' skutterudite compositions with perhaps high ZT values at room temperature. In the meantime, skutterudites are now being actively pursued for introduction into advanced thermoelectric power generation devices and systems with the potential

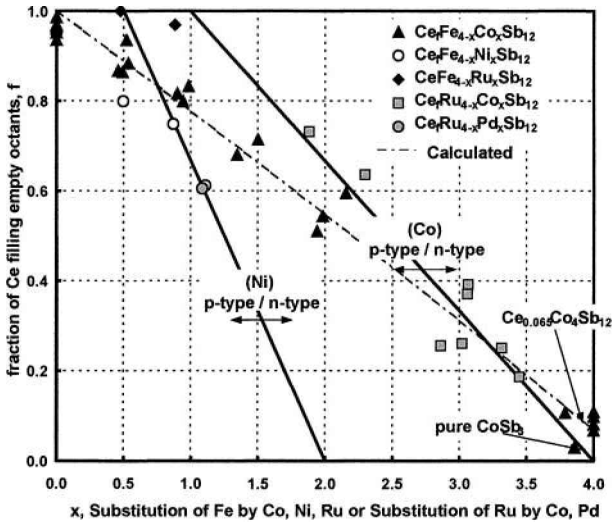

solid lines represent expected transition for Ni and Co from p-type to n-type (when VEC reaches 72), taking into account both *f* and *x* variations: when Fe is totally replaced by Co, only very small amount of Ce remains in sample ($f = 0{\cdot}07$); chain dotted line was calculated based on $CeFe_4Sb_{12}$–$Ce_{0{\cdot}065}Co_4Sb_{12}$ range of 'solid solution' compositions ($Ce_fFe_{4-x}Ni_xSb_{12}$ compositions with $x > 1{\cdot}5$ have not yet been synthesised, but it is clear that at equivalent concentrations, Ni substitution results in less Ce filling than Co substitution)

16 Ce filling fraction *f* for $Ce_fFe_{4-x}M_xSb_{12}$ samples as function of *x*, Fe substitution by M, with M = Co, Ni, and Ru

for 15% conversion efficiency in the 25–700°C temperature range.[140]

Other novel bulk materials

Clathrates

Among other materials of interest as potential new thermoelectric materials are clathrates. A clathrate material can be defined as one with a lattice that contains voids that can be filled with guest atoms or molecules. Silicon, Ge, and Sn based clathrates filled with alkaline atoms have been reported[141,142] and have recently been investigated for their thermoelectric properties.[143] They can be divided into two major groups: type I and type II. Both types have a cubic unit cell, but differ according to the number and size of the voids present in the structure. Ternary compounds have also been reported. There are numerous possible compositional, structural, and filling variations in those materials, resulting in vastly different electronic properties ranging from semimetallic to semiconducting. Recently, Nolas *et al.*[144] have measured the thermal conductivity of semiconducting $Sr_8Ga_{16}Ge_{30}$ polycrystalline samples and observed a temperature dependence typical of amorphous material. These results have triggered extensive theoretical and experimental research efforts to synthesise several of these materials and further understand their peculiar transport properties. A comprehensive review of these materials has recently appeared in the literature.[143]

The low temperature T^2 temperature dependence observed by Nolas *et al.*[144] for $Sr_8Ga_{16}Ge_{30}$ polycrystalline samples was attributed to the scattering of low frequency phonons by the Sr atoms that are loosely bonded inside the structure and are free to rattle around their atomic positions. A good indicator of the possible motion of the guest atoms is the atomic displacement parameter (ADP) that is a measure of the mean-square displacement amplitude of an atom around its equilibrium site. Unusually large ADP values have been measured for guest atoms, such as Cs and Sr in Ge based clathrates.[143] Sales *et al.* have recently proposed a model to estimate the lattice thermal conductivity based on ADP values.[145] At room temperature, the thermal conductivity of $Sr_8Ga_{16}Ge_{30}$ is close to that of amorphous Ge. Low thermal conductivity values have also been observed in other Ge based clathrates. Silicon based clathrates tend to have higher thermal conductivity values. A good thermoelectric material must combine a low lattice thermal conductivity with good electronic properties. The electronic properties of several Si, Ge, and Sn based clathrates have been measured. Metallic to semiconducting behaviour can be achieved by varying the doping and/or composition. Both n- and p-type materials can be obtained by the same process. Good Seebeck coefficient values up to $-300\ \mu V\ K^{-1}$ have been achieved. To date, the best dimensionless figure of merit ZT obtained for n-type clathrate compounds is about 0·34 with a projected value >1 above 700 K. The ability of engineering clathrate compounds with glass-like thermal conductivity combined with their relatively good electronic properties has ranked clathrates among PGEC materials, although full decoupling between their electronic and thermal properties remains to be demonstrated in these materials. Nevertheless, the encouraging results obtained to date combined with the numerous options for optimisation warrant further investigations of these interesting materials.

β-Zn_4Sb_3

Another material re-investigated recently for thermoelectric power generation is β-Zn_4Sb_3 with a hexagonal rhombohedric crystal structure, and space group $R3C$, as shown in Fig. 17. Caillat *et al.*[146] have measured the thermal conductivity of polycrystalline β-Zn_4Sb_3 samples. The lattice thermal conductivity is nearly temperature independent between 300 and 650 K, with a room temperature lattice thermal conductivity of $0{\cdot}65\ W\ m^{-1}\ K^{-1}$ at 300 K, nearly 2 times lower than that of Bi_2Te_3 alloys. This remarkably low value and unusual temperature dependence (a $1/T$ temperature dependence is usually observed) can be attributed to the relatively complex crystal structure, as well as the presence of vacancies in the lattice. The electronic transport properties are typical of a semimetal with low electrical resistivity that increases with increasing temperature. The Seebeck coefficient also increases with increasing temperature and peaks at 675 K with a value of about $200\ \mu V\ K^{-1}$. This relatively high Seebeck value for a metal is the result of a fairly large effective mass.[146] The best ZT obtained to date on polycrystalline samples is about 1·4 at 675 K (Fig. 2).[146] Above 765 K, β-Zn_4Sb_3 transforms into γ-Zn_4Sb_3 that has poorer thermoelectric properties. Band structure calculations[147] predict a metallic behaviour with improved thermoelectric performance

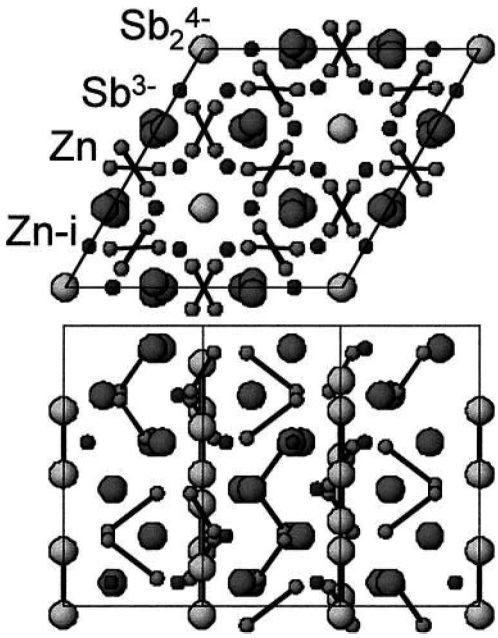

17 Schematic representation of Zn_4Sb_3 crystal structure illustrating various Sb and Zn atomic sites

for lower doping levels. Little success has however been obtained experimentally to optimise the doping level of this compound. β-Zn_4Sb_3 forms a full range of solid solutions with the isostructural compound Cd_4Sb_3. Low temperature thermal conductivity measurements on $Zn_{4-x}Cd_xSb_3$ mixed crystals showed a nearly temperature independent variation of the thermal conductivity, which is lower than for β-Zn_4Sb_3 (Ref. 148) mostly due to point defect scattering. $Zn_{4-x}Cd_xSb_3$ mixed crystals appear to be less stable than β-Zn_4Sb_3 itself and a ZT maximum of 1·4 at about 400 K was obtained for these mixed crystals. Efforts to incorporate β-Zn_4Sb_3 into advanced, high efficiency thermoelectric unicouples are in progress.[149] Further optimisation of the properties of these compounds is limited because of the difficulties to dope them and the restricted compositional variations possible.

Half-Heusler intermetallic compounds

Half-Heusler intermetallic compounds with the general formula MNiSn (M = Zr, Hf, Ti) have also attracted considerable interest as potential new thermoelectric materials.[150] These materials possess the MgAgAs structure and are closely related to the full Heusler compounds MNi_2Sn which are metals. Replacing one Ni atom by an ordered lattice of vacancies leads to a gap formation in the density of states and to a semiconducting character with band gap values on the order of 0·1 to 0·2 eV. As a result of the large electron effective mass in these materials, high Seebeck coefficients are typically obtained at 300 K and higher. Effective masses of 2–3 m_0 were estimated by Uher *et al.*[151] for ZrNiSn, and Seebeck coefficients as high as $-300\ \mu V\ K^{-1}$ were measured at 300 K for this material. It was originally suggested by Cook *et al.*[152] that these materials might be good thermoelectric materials, considering their combination of low electrical resistivity with large Seebeck coefficient values. Large power factors on the order of 25–30 $\mu W\ cm^{-1}\ K^{-2}$ have since been experimentally obtained for several of these materials, e.g. ZrNiSn and HfNiSn. The impact on the electronic properties of compositional variations and/or atomic substitutions on the various sublattices has been investigated, showing that both doping level and conductivity type can be altered. While the power factors are promising, the thermal conductivity of ternary compounds, such as ZrNiSn and HfNiSn, is rather high. The total thermal conductivity (which is essentially the lattice thermal conductivity for these materials) ranges from 5·9 to 17 $W\ m^{-1}\ K^{-1}$ for ZrNiSn.[151] The spread in the values was primarily due to the difference of structural quality introduced, for example, by annealing the samples. Attempts to reduce the lattice thermal conductivity of these materials using mass-defect scattering on the various sublattices were made. Although lattice thermal conductivity values of 5–6 $W\ m^{-1}\ K^{-1}$ were obtained for alloys, these values are still too high compared to those obtained for state of the art thermoelectric alloys, such as Bi_2Te_3 alloys. Efforts should therefore focus on further reducing the lattice thermal conductivity of these materials that otherwise possess impressive electronic properties that can be tuned through doping and alloying. Possible schemes for reducing the thermal conductivity may however be somewhat limited apart from the introduction of point defect scattering, since these materials are not 'cage-like' materials, such as skutterudites or clathrates. Most transport property measurements on half-Heusler alloys to date have been limited to low temperatures but these materials may actually be quite interesting at temperatures up to 800–900 K, considering that they typically behave as semimetals at temperatures below 300 K and semiconductors above that temperature. Transport property measurements above 300 K would therefore be of interest to fully assess the potential of these materials for thermoelectric applications.

Complex chalcogenides

While several materials with $ZT > 1$ have been identified above room temperature, there is a great need for new thermoelectric materials with $ZT > 1$ for cooling applications. At and below room temperature, only two materials have been known for many years to have decent thermoelectric properties: Bi–Sb and Bi_2Te_3 alloys. Past studies suggest new low temperature semiconducting thermoelectric materials are likely to be found in narrow band gap materials.[14]

An extensive effort at Michigan State University has focused on a number of new chalcogenides composed mostly of heavy elements. As a result, a number of potential new materials for low temperature thermoelectric applications have been identified. A comprehensive review of these materials has recently appeared in the literature.[153] A number of complex phases have been prepared preferably by a flux technique and several new compounds have been identified. Among the materials investigated are the sulphides $KBi_{6.33}S_{10}$ and $K_2Bi_8S_{13}$, the selenides β-$K_2Bi_8Se_{13}$ and $K_{2.5}Bi_{8.5}Se_{14}$, $A_{1+x}Pb_{4-2x}Bi_{7+x}Se_{15}$ (A = K, Rb) compounds, and the tellurides A/Bi/Te

and A/Pb/Bi/Te. A common feature for most of these materials is their low thermal conductivity, comparable or even lower than that of Bi_2Te_3 alloys. Many of these compounds show very anisotropic transport properties. Perhaps the most promising compound identified to date is $CsBi_4Te_6$. This compound has a layered anisotropic structure with Cs ions between $[Bi_4Te_6]$ layers. The ADPs of the Cs ions are 1·6 times greater than those of the Bi and Te atoms. Crystals of $CsBi_4Te_6$ grow with a needlelike morphology and are stable in air and water. The crystals are amenable to doping and SbI_3, BiI_3, and In_2Te_3 have been successfully used to optimise the carrier concentration of this material. The power factor can be maximised through doping and a maximum power factor value of about 50 $\mu W\,cm^{-1}\,K^{-2}$ was obtained at 185 K for the p-type material.[153] The total thermal conductivity along the growth axis is about 1·5 $W\,m^{-1}\,K^{-1}$ at 300 K and is essentially constant down to 100 K. This atypical temperature dependence suggests again that the rattling Cs ions significantly contribute to phonon scattering in this compound. The best ZT to date obtained along the needle direction is 0·82 for the p-type material (Fig. 2), slightly better than p-type Bi_2Te_3 at this temperature. The In_2Te_3 'doped' n-type material has poorer thermoelectric properties. Nevertheless, p-type $CsBi_4Te_6$ is the first compound identified in the low temperature range to match or even outperform Bi_2Te_3 alloys. Whether or not this compound can be further optimised through doping and/or alloying will need to be determined in the future as well as its mechanical stability under thermal stresses to warrant its practical use in devices.

Pentatelluride materials such as $HfTe_5$ and $ZrTe_5$ and their alloys have been considered promising new thermoelectric materials at low temperatures because of their relatively large Seebeck coefficient values at low temperatures which, combined with relatively low electrical resistivity values, result in large power factor values.[154] Their electronic properties can be tuned through alloying and doping, but the challenge for these materials is to reduce their lattice thermal conductivity. Another challenge lies in the very anisotropic nature of these materials that requires the growth and characterisation of single crystals for transport properties. Single crystal whiskers were obtained by a vapour transport technique, but measurements on these small crystals offer great challenges. Further investigations will be required to determine whether or not the transport properties of these materials can be further optimised and if thermal conductivity values close to those for state of the art thermoelectric materials can be obtained without significantly degrading their electronic properties.

Special challenges in materials synthesis and characterisation

Compared to semiconductor materials for electronic and optoelectronic devices, thermoelectric materials impose different sets of materials requirements, which in turn create new challenges in their materials synthesis and characterisation. Some of these special challenges will be briefly discussed here.

Thermoelectric materials require high doping with carrier concentrations of $\sim 10^{19}\,cm^{-3}$. Careful optimisation of the doping concentration is necessary. Thus an experimental thermoelectric research programme must be prepared in the synthesis and optimisation, as well as fast characterisation turnaround capability.

Most thin films in electronic devices are on the order of submicrometres in the film thickness. Thermoelectric thin films should typically be thicker, both for characterisation purposes and for device applications. For thermoelectric devices in the cross-plane direction, films thicker than a few micrometres or even much thicker are desirable in terms of sustaining a reasonable temperature differential. For thermoelectric devices intended for use for in-plane transport applications, the reverse heat flow from the supporting substrate must be minimised. This means either the removal of the substrate or depositing very thick films. Thus, both in-plane and cross-plane devices demand relatively thick films, while quantum or classical size effects typically require individual layers of the order of several tens of angstroms. Such conflicting requirements impose a severe limit for the practical scale up of materials synthesis methods, although in research, many thin film deposition methods, such as molecular beam epitaxy, metallo-organic chemical vapour deposition, pulsed laser deposition, and sputtering, are all being explored.

Thermoelectric materials employ relatively large numbers of alloy compositions. For example, $Si_{0·8}Ge_{0·2}$ is typically used in bulk thermoelectric generators. For comparison, electronic devices based on SiGe alloys, such as heterojunction bipolar transistors, use 1–5%Ge concentration. A larger concentration of Ge is required for thermoelectrics applications to create more thermal conductivity reduction. Even in superlattices, a relatively large equivalent Ge concentration is needed for sufficient thermal conductivity reduction. For superlattices made of materials with a large mismatch in their lattice constants, buffer layers are needed. To grow 20/20 Å Si/Ge superlattices, for example, graded buffer layers of SiGe alloys from 1 to 5 μm with continuously varying Ge concentrations have been used. These buffer layers complicate the characterisation and usually degrade the device performance.

The characterisation of thermoelectric properties of potentially interesting thermoelectric materials, particularly samples consisting of low-dimensional structures, imposes an even greater challenge. Even for bulk materials, thermal conductivity measurements are never easy and are prone to large uncertainty. For low-dimensional structures, thermal conductivity measurements are much trickier. The most widely used method for cross-plane thermal conductivity measurements is the 3ω method that relies on the deposition of small heaters that also act as temperature sensors.[87] The principle of the 3ω method is simple, but when applied to specific low-dimensional structures, it can be quite involved, due to the following factors.

1. Thermoelectric films are conducting, thus an insulator is needed for electrical isolation between the sensor and the sample. The insulator has unknown

thermal conductivity. Often, a differential method is used.[155]

2. Superlattices are grown on substrates and buffers, whose properties are not exactly known. Although the principle of the 3ω method allows the measurements to be made on the thermal conductivity of the substrate, the determination of a high thermal conductivity substrate is actually subject to quite large uncertainties. The buffer layers typically have unknown and anisotropic thermal conductivities that cannot be easily determined.

3. Superlattices also have anisotropic properties, and thus care must be taken to ascertain which direction is being measured. Through careful modelling, both the in-plane and cross-plane direction thermal conductivity can be determined.[40] Several other factors, such as the thermal property contrast between the film and the substrate and the film heat capacity effects, are discussed in detail by Borca-Tasciuc *et al.*[155] In addition to the 3ω method, other methods that have been used often are the ac calorimetry method for determining the thermal conductivity along the film plane direction,[156] and the pump-and-probe method for determining the cross-plane thermal conductivity.[80]

The determination of the Seebeck effect is usually not considered to be a big challenge for bulk materials, but it can be quite tricky for superlattices that are grown on substrates and buffers because the substrate may make a large contribution to the overall measured properties. Although corrections can be made based on simple circuit theory, there is no strong evidence that such corrections are reliable. Several methods have been attempted in the past for measuring the in-plane Seebeck coefficient and conductivity of superlattices, by removing the substrate or by growing the samples on insulators.[28,36,157,158] Even for samples grown on insulators, such as Si/Ge superlattices grown on silicon-on-insulator substrates, the additional contributions of the buffer and of the silicon layer must be taken into account. In the cross-plane direction, direct measurements of the Seebeck coefficient have only been reported very recently.[159] One can appreciate the difficulties involved by examining equation (1), which requires measurements of both the temperature difference and the voltage drop across two equivalent points. In the cross-plane direction, this measurement becomes extremely challenging, since the thickness of the film is typically on the order of 1–10 μm. The ZT values in the cross-plane direction for Bi_2Te_3/Sb_2Te_3 superlattices[11] have been measured using the transient Harman method.[1]

It should be emphasised that all the measurements should be done in the same direction and preferably also on the same sample. For low-dimensional structures, this has proven to be a very difficult goal to achieve. For these reasons, the ZT values of low-dimensional structures plotted Fig. 2 should be further confirmed.

Concluding remarks

In summary, the recent resurgence in thermoelectric materials research has led to quite a large increase in ZT values and significant new insights into thermoelectric transport in both low-dimensional and bulk materials. However, there is much left to be done, in new materials syntheses, characterisation, physical understanding, and device fabrication. It is hoped that this review will arouse broader interest in thermoelectrics research from the materials research community. Meanwhile, the authors would like to emphasise that thermoelectric materials research is a multidisciplinary endeavour and requires close collaboration between researchers in different fields to address issues in materials, theory, characterisation, and eventually, devices.

Acknowledgements

Two of the authors (GC and MSD) gratefully acknowledge their collaborators in thermoelectric research, including Professors R. Gronsky, J.-P. Issi, T. D. Sands, K. L. Wang, Dr J. Heremans, and T. Harman, and contributions from all students in their respective research groups. The authors are grateful for support for this work by DoD MURI: N00014–97–1–0516 (GC and MSD), US Navy Contract N00167–98–K–0024 (MSD), DARPA Contract N66001–00–1–8603 (MSD), DARPA HERETIC Project (J-PF and GC), JPL: 004736–001 (J-PF and GC), and NSF Grant DMR 01–16042 (MSD).

References

1. H. J. GOLDSMID: 'Thermoelectric refrigeration'; 1964, New York, Plenum Press.
2. A. F. IOFFE: 'Semiconductor thermoelements and thermoelectric cooling'; 1957, London, Infosearch Ltd.
3. G. N. HATSOPOULOS and J. KAYE: *J. Appl. Phys.*, 1958, **29**, 1124–1126.
4. G. D. MAHAN: *J. Appl. Phys.*, 1994, **76**, 4362–4366.
5. G. SLACK: in 'CRC handbook of thermoelectrics', (ed. D. M. Rowe), 407–440; 1995, Boca Raton, CRC Press.
6. L. D. HICKS and M. S. DRESSELHAUS: *Phys. Rev. B*, 1993, **47**, 12727–12731.
7. T. C. HARMAN, P. J. TAYLOR, D. L. SPEARS, and M. P. WALSH: *J. Electron. Mater.*, 2000, **29**, L1–L4.
8. B. Y. MOYZHES and V. NEMCHINSKY: Proc. Int. Conf. on 'Thermoelectrics', ICT'92, 1992, 232–235 (*Appl. Phys. Lett.*, 1998, **73**, 1895–1897).
9. A. SHAKOURI and J. E. BOWERS: *Appl. Phys. Lett.*, 1997, **71**, 1234.
10. G. D. MAHAN: *Semicond. Semimet.*, 2001, **71**, 157–174.
11. R. VENKATASUBRAMANIAN: *Semicond. Semimet.*, 2001, **71**, 175–201.
12. G. CHEN: *Semicond. Semimet.*, 2001, **71**, 203–259.
13. T. M. TRITT (ed.): in 'Recent trends in thermoelectric materials research', *Semicond. Semimet.*, 2001, **69**–**71**.
14. G. D. MAHAN: *Solid State Phys.*, 1998, **51**, 81–157.
15. G. S. NOLAS, D. T. MORELLI and T. M. TRITT: *Ann. Rev. Mater. Sci.*, 1999, **29**, 89–116.
16. F. J. DISALVO: *Science*, 1999, **285**, (5428), 703–706.
17. G. S. NOLAS and G. A. SLACK: *Am. Sci.*, 2001, **89**, (2), 136–141.
18. Proc. Int. Conf. on 'Thermoelectrics': e.g. ICT'97 (IEEE Cat. no. 97TH8291), ICT'98 (IEEE Cat. no. 98TH8365), ICT'99 (IEEE Cat. no. 99TH8407), ICT'00 (Babrow Press, Wales, UK, ISBN 0951928627), ICT'01 (IEEE Cat. no. 01TH8589).
19. MRS Proceedings on Thermoelectrics: **478** (1997), **545** (1998), **626** (2000); Warrendale, PA, Materials Research Society.
20. N. W. ASCHROFT and N. D. MERMIN: 'Solid state physics'; 1976, Forth Worth, Saunders College Publishing.
21. M. S. DRESSELHAUS, Y.-M. LIN, S. B. CRONIN, O. RABIN, M. R. BLACK, G. DRESSELHAUS, and T. KOGA: *Semicond. Semimet.*, 2001, **71**, 1–121.
22. J. GOLDSMID: in Proc. 17th Int. Conf. on 'Thermoelectrics', ICT'98, 1998, 25–28 (IEEE Cat. no. 98TH8365).
23. D. J. SINGH: *Semicond. Semimet.*, 2001, **70**, 125–178.

24. L. D. HICKS and M. S. DRESSELHAUS: *Phys. Rev. B*, 1993, **47**, 16631–16634.
25. L. D. HICKS: 'The effect of quantum-well superlattices on the thermo-electric figure of merit', PhD thesis, MIT, June 1996.
26. T. KOGA, T. C. HARMAN, X. SUN, and M. S. DRESSELHAUS: *Phys. Rev. B*., 1999, **60**, 14286–14293.
27. L. D. HICKS, T. C. HARMAN, and M. S. DRESSELHAUS: *Phy. Rev. B*., 1996, **53**, 10493–10496.
28. X. SUN, S. B. CRONIN, J. L. LIU, K. L. WANG, T. KOGA, M. S. DRESSELHAUS, and G. CHEN: Proc. 18th Int. Conf. on 'Thermoelectrics', ICT'99, 1999, 652–655 (IEEE Cat. no. 99TH8407).
29. T. KOGA, S. B. CRONIN, M. S. DRESSELHAUS, J. L. LIU, and K. L. WANG: *Appl. Phys. Lett*., 1999, **77**, 1490–1492
30. T. C. HARMAN, D. L. SPEARS, D. R. CALAWA, S. H. GROVES, and M. P. WALSH: Proc. 16th Int. Conf. on 'Thermoelectrics', ICT'97, 1997, 416–423 (IEEE Cat. no. 97TH829).
31. T. C. HARMAN, D. L. SPEARS, and M. P. WALSH: *J. Electron. Mater. Lett*., 1999, **28**, L1–L4.
32. J. O. SOFO and G. D. MAHAN: *Appl. Phys. Lett*., 1994, **65**, 2690–2692.
33. D. A. BROIDO and T. L. REINECKE: *Phys. Rev. B*, 1995, **51**, 13797–13800.
34. T. KOGA: 'Concept and applications of carrier pocket engineering to design useful thermoelectric materials using superlattice structures', PhD thesis, Harvard University, June 2000.
35. T. KOGA, X. SUN, S. B. CRONIN, and M. S. DRESSELHAUS: *Appl. Phys. Lett*., 1998, **73**, 2950–2952.
36. T. KOGA, X. SUN, S. B. CRONIN, and M. S. DRESSELHAUS: *Appl. Phys. Lett*., 1999, **75**, 2438–2440.
37. T. YAO: *Appl. Phys. Lett*., 1987, **51**, 1798–1800.
38. G. CHEN, C. L. TIEN, X. WU, and J. S. SMITH: *J. Heat Transf*., 1994, **116**, 325–331.
39. X. Y. YU, G. CHEN, A. VERMA, and J. S. SMITH: *Appl. Phys. Lett*., 1995, **67**, 3554–3556; 1996, **68**, 1303.
40. W. L. LIU, T. BORCA-TASCIUC, G. CHEN, J. L. LIU, and K. L. WANG: *J. Nanosci. Nanotechnol*., 2001, **1**, 39–42.
41. H. BEYER, J. NURNUS, H. BOTTNER, L. LAMBRECHT, T. ROCH, and G. BAUER: *Appl. Phys. Lett*., 2002, **80**, 1216–1218.
42. T. C. HARMAN, P. J. TAYLOR, M. P. WALSH, and B. E. LAFORGE: *Science*, 2002, **297**, 2229.
43. X. SUN, Z. ZHANG, and M. S. DRESSELHAUS: *Appl. Phys. Lett*., 1999, **74**, 4005–4007.
44. Z. B. ZHANG: 'Fabrication, characterization and transport properties of bismuth nanowire systems', PhD thesis, MIT, February 1999.
45. Y.-M. LIN: 'Fabrication, characterization and theoretical modeling of Te-doped Bi nanowire systems for thermoelectric applications', MS thesis, MIT, January 2000.
46. Z. ZHANG, X. SUN, M. S. DRESSELHAUS, J. Y. YING, and H. HEREMANS: *Appl. Phys. Lett*., 1998, **73**, 1589–1591.
47. J. HEREMANS, C. M. TRUSH, Z. ZHANG, X. SUN, M. S. DRESSELHAUS, J. Y. YING, and D. T. MORELLI: *Phys. Rev. B*, 1998, **58**, R10091–R10095.
48. Z. ZHANG, X. SUN, M. S. DRESSELHAUS, J. Y. YING, and J. HEREMANS: *Phys. Rev. B*, 2000, **61**, 4850–4861.
49. J. HEREMANS, C. M. TRUSH, Y.-M. LIN, S. CRONIN, Z. ZHANG, M. S. DRESSELHAUS, and J. F. MANSFIELD: *Phys. Rev. B*, 2000, **61**, 2921–2930.
50. Y. M. LIN, X. SUN, and M. S. DRESSELHAUS: *Phys. Rev. B*, 2000, **62**, 4610–4623.
51. B. LENOIR, M. CASSART, J. P. MICHENAUD, H. SHERRER, and S. SHERRER: *J. Phys. Chem. Solids*, 1996, **57**, 88–89.
52. O. RABIN, Y. M. LIN, and M. S. DRESSELHAUS: *Appl. Phys. Lett*., 2001, **79**, 81–83.
53. Y.-M. LIN, S. B. CRONIN, O. RABIN, J. Y. YING, and M. S. DRESSELHAUS: *Appl. Phys. Lett*., 2001, **79**, 677–679.
54. L. W. WHITLOW and T. HIRANO: *J. Appl. Phys*., 1995, **78**, 5460–5466.
55. R. J. RADTKE, H. EHRENREICH, and C. H. GREIN: *J. Appl. Phys*., 1999, **86**, 3195–3198.
56. G. D. MAHAN: *J. App. Phys*., 1994, **76**, 4362–4366.
57. G. D. MAHAN and L. M. WOODS: *Phys. Rev. Lett*., 1998, **80**, 4016–4019.
58. G. D. MAHAN, J. O. SOFO, and M. BARTKOWIAK: *J. Appl. Phys*., 1998, **83**, 4683–4689.
59. C. B. VINING and G. D. MAHAN: *J. Appl. Phys*., 1999, **86**, 6852–6853.
60. N. M. MISKOVSKY and P. H. CUTLER: *Appl. Phys. Lett*., 1999, **75**, 2147–2149.
61. A. N. KOROTKOV and K. K. LIKHAREV: *Appl. Phys. Lett*., 1999, **75**, 2491–2493.
62. T. ZENG and G. CHEN: Proc. Int. Mech. Eng. Congress and Exhibition, ASME HTD–Vol. 366–2, 2000, 361–372.
63. T. ZENG and G. CHEN: *J. Appl. Phys*., 2002, **92**, 3152.
64. G. CHEN and T. ZENG: *Microscale Thermophys. Eng*., 2001, **5**, 71–88.
65. A. SHAKOURI, C. LABOUNTY, J. PIPREK, P. ABRAHAM, and J. E. BOWERS: *Appl. Phys. Lett*., 1999, **74**, 88–89.
66. G. H. ZENG, A. SHAKOURI, C. LA BOUNTY, G. ROBINSON, E. CROKE, P. ABRAHAM, X. F. FAN, H. REESE, and J. E. BOWERS: *Electronics Lett*., 1999, **35**, 2146–2147.
67. X. F. FAN, G. H. ZENG, C. LABOUNTY, J. E. BOWERS, E. CROKE, C. C. AHN, S. HUXTABLE, A. MAJUMDAR, and A. SHAKOURI: *Appl. Phys. Lett*., 2001, **78**, 1580–1582.
68. X. F. FAN, G. ZENG, E. CROKE, C. LABOUNTY, C. C. AHN, D. VASHAEE, A. SHAKOURI, and J. E. BOWERS: *Electron. Lett*., 2001, **37**, 126–127.
69. C. LABOUNTY, A. SHAKOURI, P. ABRAHAM, and J. E. BOWERS: *Opt. Eng*., 2000, **39**, 2847–2852.
70. C. LABOUNTY, A. SHAKOURI, and J. E. BOWERS: *J. Appl. Phys*., 2001, **89**, 4059–4064.
71. R. TSU and R. F. GREENE: *Electrochem. Solid State Lett*., 1999, **2**, 645–647.
72. H. B. G. CASIMIR: *Physica*, 1938, **5**, 495–500.
73. C. L. TIEN and G. CHEN: in Proc. Am. Soc. Mech. Eng., ASME HTD–Vol. 227, 1992, 1–12 (*J. Heat Transf*., 1994, **116**, 799–807).
74. G. CHEN: *Ann. Rev. Heat Transf*., 1996, **7**, 1–57.
75. R. VENKATASUBRAMANIAN: *Naval Res. Rev*., 1996, **58**, 44–54.
76. R. VENKATASUBRAMANIAN, E. SILVOLA, and T. COLPITTS: *Nature*, 2001, **413**, 597–602.
77. I. YAMASAKI, R. YAMANAKA, M. MIKAMI, H. SONOBE, Y. MORI, and T. SASAKI: Proc. 17th Int. Conf. on 'Thermoelectrics', ICT'98, 1998, 210–213 (IEEE Cat. no. 98TH8365).
78. M. N. TOUZELBAEV, P. ZHOU, R. VENKATASUBRAMANIAN, and K. E. GOODSON: *J. Appl. Phys*., 2001, **90**, 763–767.
79. W. S. CAPSINSKI and H. J. MARIS: *Physica B*, 1996, **220**, 699–701.
80. W. S. CAPINSKI, H. J. MARIS, T. RUF, M. CARDONA, K. PLOOG, and D. S. KATZER: *Phys. Rev. B*, 1999, **59**, 8105–8113.
81. S. M. LEE, D. G. CAHILL, and R. VENKATASUBRAMANIAN: *Appl. Phys. Lett*., 1997, **70**, 2957–2959.
82. T. BORCA-TASCIUC, W. L. LIU, T. ZENG, D. W. SONG, C. D. MOORE, G. CHEN, K. L. WANG, M. S. GOORSKY, T. RADETIC, R. GRONSKY, T. KOGA, and M. S. DRESSELHAUS: *Superlattices Microstruct*., 2000, **28**, 119–206.
83. R. VENKATASUBRAMANIAN: *Phys. Rev. B*, 2000, **61**, 3091–3097.
84. T. BORCA-TASCIUC, D. ACHIMOV, W. L. LIU, G. CHEN, H.-W. REN, C.-H. LIN, and S. S. PEI: *Microscale Thermophys. Eng*., 2001, **5**, 225–231.
85. S. T. HUXTABLE, A. SHAKOURI, C. LABOUNTY, X. FAN, P. ABRAHAM, Y. J. CHIU, J. E. BOWERS, and A. MAJUMDAR: *Microscale Thermophys. Eng*., 2000, **4**, 197–203.
86. D. W. SONG, W. L. LIU, T. ZENG, T. BORCA-TASCIUC, G. CHEN, C. CAYLOR, and T. D. SANDS: *Appl. Phys. Lett*., 2000, **77**, 3854–3856.
87. S. M. LEE and D. G. CAHILL: *J. Appl. Phys*., 1997, **81**, 2590–2595.
88. P. HYLDGAARD and G. D. MAHAN: *Phys. Rev. B*, 1997, **56**, 10754–10757.
89. S. TAMURA, Y. TANAKA, and H. J. MARIS: *Phys. Rev. B*, 1999, **60**, 2627–2630.
90. W. E. BIES, R. J. RADTKE, and H. EHRENREICH: *J. Appl. Phys*., 2000, **88**, 1498–1503.
91. A. A. KISELEV, K. W. KIM, and M. A. STROSCIO: *Phys. Rev. B*, 2000, **62**, 6896–6899.
92. B. YANG and G. CHEN: *Microscale Thermophys. Eng*., 2001, **5**, 107–116.
93. A. BALANDIN and K. L. WANG: *J. App. Phys*., 1998, **84**, 6149–6153.
94. G. CHEN: *J. Heat Transf*., 1997, **119**, 220–229 (Proc. 1996 Nat. Heat Transfer Conf., ASME HTD–Vol. 323, 1996, 121–130).
95. P. HYLDGAARD and G. D. MAHAN: in 'Thermal conductivity', Vol. 23, 172–181; 1996, Lancaster, Technomic.
96. G. CHEN and M. NEAGU: *Appl. Phys. Lett*., 1997, **71**, 2761–2763.
97. G. CHEN: *Phys. Rev. B*, 1998, **57**, 14958–14973 (*see* also Proc. 1996 Int. Mech. Eng. Congr., 1996, DSC–Vol. 59, 13–24).
98. G. CHEN: *J. Heat Transf*., 1999, **121**, 945–953.
99. K. E. GOODSON and Y. S. JU: *Ann. Rev. Mater*., 1999, **29**, 261–293.
100. K. E. GOODSON: *Ann. Rev. Heat Transf*., 1995, **6**, 323–353.

101. G. A. SLACK: *Solid State Phys.*, 1979, **34**, 1–71.
102. D. G. CAHILL, S. K. WATSON, and R. O. POHL: *Phys. Rev. B*, 1992, **46**, 6131–6140.
103. H. GRILLE, K. KARCH, and F. BECHSTEDT: *Physica B*, 1996, **220**, 690–692.
104. R. S. PRASHER and P. E. PHELAN: *J. Heat Transf.*, 1998, **120**, 1078–1086.
105. B. YANG and G. CHEN: *Phys. Low-Dimensional Struct. J.*, 2000, **5/6**, 37–48.
106. J. D. WALKER, D. M. KUCHTA, and J. S. SMITH: *Appl. Phys. Lett.*, 1991, **59**, 2079–2081.
107. L. I. ARUTYUNYAN, V. N. BOGOMOLOV, N. F. KARTENKO, D. A. KURDYUKOV, V. V. POPOV, A. V. PROKOF'EV, I. A. SMIRNOV, and N. V. SHARENKOVA: *Phys. Solid State*, 1997, **39**, 510–514.
108. D. W. SONG, W.-N. SHEN, T. ZENG, W. L. LIU, G. CHEN, B. DUNN, C. D. MOORE, M. S. GOORSKY, R. RADETIC, and R. GRONSKY: ASME HTD–Vol. 364–1, 1999, 339–344.
109. S. G. VOLZ and G. CHEN: *Appl. Phys. Lett.*, 1999, **75**, 2056–2058.
110. S. G. WALKAUSKAS, D. A. BROIDO, K. KEMPA, and T. L. REINECKE: *J. Appl. Phys.*, 1999, **85**, 2579–2582.
111. P. KIM, L. SHI, A. MAJUMDAR, and P. L. MCEUEN: *Phys. Rev. Lett.*, 2001, **87**, 215502-1–5502-4.
112. T. CAILLAT, A. BORSHCHEVSKY, and J.-P. FLEURIAL: Proc. 7th Int. Conf. on 'Thermoelectrics', (ed. K. Rao); Arlington, TX, University of Texas. 98–101 1993.
113. J.-P. FLEURIAL, T. CAILLAT, and A. BORSHCHEVSKY: Proc. 13th Int. Conf. on 'Thermoelectrics', 209–211; 1994, New York, AIP Press no. 316.
114. C. UHER: *Semicond. Semimet.*, 2001, **69**, 139–253.
115. S. RUNDQVIST and N.-O. ERSSON: *Arkiv for Kemi*, 1968, **30**, 103–114.
116. W. JEITSCHKO and D. BRAUN: *Acta Crystallogr.*, 1977, **B33**, 3401–3406.
117. J.-P. FLEURIAL, T. CAILLAT, and A. BORSHCHEVSKY: Proc. 16th Int. Conf. on 'Thermoelectrics', 1997, 1–11 (IEEE Cat. no. 97TH8291).
118. G. P. MEISNER, M. S. TORIKACHVILI, K. N. YANG, M. B. MAPLE, and R. P. GUERTIN: *J. Appl. Phys.*, 1985, **57**, 3073–3075.
119. D. JUNG, M. H. WHANGBO, and S. ALVAREZ: *Inorganic Chem.*, 1990, **29**, 2252–2255.
120. F. GRANDJEAN, A. GÉRARD, D. J. BRAUN, and W. JEITSCHKO: *J. Phys. Chem. Solids*, 1984, **45**, 877–886.
121. N. T. STETSON, S. M. KAUZLARICH, and H. HOPE: *J. Solid State Chem.*, 1991, **91**, 140–147.
122. D. J. BRAUN and W. JEITSCHKO: *J. Less-Common Met.*, 1980, **76**, 33–40.
123. M. E. DANEBROCK, C. B. H. EVERS, and W. JEITSCHKO: *J. Phys. Chem. Solids*, 1996, **57**, 381–387.
124. D. T. MORELLI, T. CAILLAT, J.-P. FLEURIAL, A. BORSHCHEVSKY, J. VANDERSANDE, B. CHEN, and C. UHER: *Phys. Rev. B*, 1995, **51**, 9622–9628.
125. T. CAILLAT, A. BORSHCHEVSKY, and J.-P. FLEURIAL: *J. Appl. Phys.*, 1996, **80**, 4442–4449.
126. A. WATCHARAPASORN, R. C. DEMATTEI, R. S. FEIGELSON, T. CAILLAT, A. BORSHCHEVSKY, G. J. SNYDER, and J.-P. FLEURIAL: *J. Appl. Phys.*, 1999, **86**, 6213–6217.
127. T. CAILLAT, J.-P. FLEURIAL, and A. BORSCHEVSKY: *J. Cryst. Growth*, 1996, **166**, 722–726.
128. H. ANNO, K. MATSUBARA, Y. NOTOHARA, T. SAKAKIBARA, and H. TASHIRO: *J. Appl. Phys.*, 1999, **86**, 3780–3786.
129. R. P. CHASMAR and R. J. STRATTON: *Electron. Contrib.*, 1959, **7**, 52.
130. D. J. SINGH, I. I. MAZIN, S. G. KIM, and L. NORDSTROM: MRS Symp. Proc. **478**, 187; 1997, Warrendale, PA, Materials Research Society.
131. J. O. SOFO and G. D. MAHAN: MRS Symp. Proc. **545**, 315; 1999, Warrendale, PA, Materials Research Society.
132. G. A. SLACK, J.-P. FLEURIAL, and T. CAILLAT: *Naval Res. Rev.*, 1996, **58**, 23–30.
133. G. S. NOLAS, V. G. HARRIS, T. M. TRITT, and G. A. SLACK: *J. Appl. Phys.*, 1996, **80**, 6304–6308.
134. J.-P. FLEURIAL, A. BORSHCHEVSKY, T. CAILLAT, D. T. MORELLI, and G. P. MEISNER: Proc. 15th Int. Conf. on 'Thermoelectrics', 1996, 91–95 (IEEE Cat. no. 96TH8169).
135. B. C. SALES, D. MANDRUS, and R. K. WILLIAMS: *Science*, 1996, **22**, 1325–1328.
136. D. J. BRAUN and W. JEITSCHKO: *J. Less-Common Met.*, 1980, **72**, 147–156.
137. M. FORNARI and D. J. SINGH: *Appl. Phys. Lett.*, 1999, **74**, 3666–3668.
138. H. TAKIZAWA, K. MIURA, M. ITO, T. SUZUKI, and T. ENDO: *J. Alloy. Compd.*, 1999, **282**, 79–83.
139. H. UCHIDA, V. CRNKO, H. TANAKA, A. KASAMA, and K. MATSUBARA: Proc. 17th Int. Conf. on 'Thermoelectrics', ICT'98, 1998, 330 (IEEE Cat. no. 98TH8365).
140. T. CAILLAT, J.-P. FLEURIAL, G. J. SNYDER, A. ZOLTAN, D. ZOLTAN, and A. BORSHCHEVSKY: Proc. 34th Intersociety Energy Conversion Engineering Conf. IECE99CD, 1999–01–2567, 1–7.
141. C. CROS, M. POUCHARD, P. HAGENMULLER, and J. S. KASPER: *Bull. Soc. Chim. Fr.*, 1968, **7**, 2737.
142. J. GALLMEIER, H. SCHÄFFER, and A. WEISS: *Z. Naturforsch.*, 1969, **24B**, 665.
143. G. S. NOLAS, G. A. SLACK, and S. B. SCHUJMAN: *Semicond. Semimet.*, 2001, **69**, 255–300.
144. G. S. NOLAS, J. L. COHN, G. A. SLACK, and S. B. SCHUJMAN: *Appl. Phys. Lett.*, 1998, **73**, 178–180.
145. B. C. SALES, B. C. CHAKAMOUKOS, D. MANDRUS, and J. W. SHARP: *J. Solid State Chem.*, 1999, **146**, 528–532.
146. T. CAILLAT, J.-P. FLEURIAL, and A. BORSHCHEVSKY: *J. Phys. Chem. Solids*, 1997, **58**, 1119–1125.
147. S.-G. KIM, I. I. MAZIN, and D. J. SINGH: *Phys. Rev. B*, 1998, **57**, 6199–6203.
148. T. CAILLAT, J.-P. FLEURIAL, and A. BORSHCHEVSKY: MRS Symp. Proc. **478**, 103; 1997, Warrendale, PA, Materials Research Society.
149. T. CAILLAT, J.-P. FLEURIAL, G. J. SNYDER, A. ZOLTAN, D. ZOLTAN, and A. BORSHCHEVSKY: Proc. 17th Int. Conf. on 'Thermoelectrics', ICT'99, 473–476 (IEEE Cat. no. 99TH8407).
150. S. J. POON: *Semicond. Semimet.*, 2001, **70**, 37–76.
151. C. UHER, J. YANG, S. HU, D. T. MORELLI, and G. P. MEISNER: *Phys. Rev. B.*, 1999, **59**, 8615–8621.
152. B. A. COOK, J. L. HARRINGA, Z. S. TAN, and W. A. JESSER: Proc. 15th Int. Conf. on 'Thermoelectrics', ICT'96, 1996, 122–127 (IEEE Cat. No. 97TH8169).
153. M. G. KANATZIDIS: *Semicond. Semimet.*, 2001, **69**, 51–100.
154. R. T. LITTLETON, T. M. TRITT, C. R. FEGER, J. KOLIS, M. L. WILSON, and M. MARONE: *Appl. Phys. Lett.*, 1998, **72**, 2056–2058.
155. T. BORCA-TASCIUC, R. KUMAR, and G. CHEN: *Rev. Sci. Instr.*, 2001, **72**, 2139–2147.
156. I. HATTA: *Int. J. Thermophys.*, 1990, **11**, 293–303.
157. T. BORCA-TASCIUC, W. L. LIU, J. L. LIU, K. L. WANG, and G. CHEN: Proc. 35th Nat. Heat Transfer Conf., NHTC'01, paper no. NHTC2001–20097; 2001, New York, ASME Press.
158. G. CHEN, B. YANG, W. L. LIU, T. BORCA-TASCIUC, D. SONG, D. ACHIMOV, M. S. DRESSELHAUS, J. L. LIU, and K. L. WANG: Proc. 20th Int. Conf. on 'Thermoelectrics', ICT'01, 2001, 30–34 (IEEE Cat. no. 01TH8589).
159. B. YANG, J. L. LIU, K. L. WANG, and G. CHEN: *Appl. Phys. Lett.*, 2002, **80**, 1758–1760.